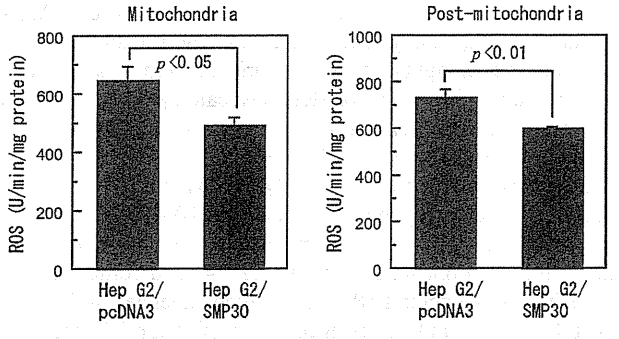

Fig. 2. ROS Formation in the Mitochondrial and Post-mitochondrial Fractions of the Hep G2/SMP30 and Hep G2/pcDNA3 Mock-Transfected Control Cells

ROS levels were measured by applying oxidation-sensitive C400 fluorescent dye to mitochondrial and post-mitochondrial fractions as described in Materials and Methods. The changes of fluorescence intensity from 30 to 60 min were normalized by time and protein concentration. Values are expressed as mean±S.D. of five different experiments.

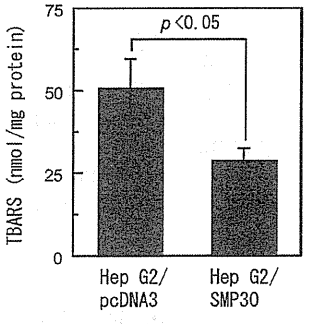

Fig. 3. Lipid Peroxidation Level of the Hep G2/SMP30 and Hep G2/pcDNA3 Mock-Transfected Control Cells

The amount of lipid peroxides was calculated as TBARS products of lipid peroxidation as described in Materials and Methods. Values are expressed as mean±S.D. of five different experiments.

cells, the formation of ROS was a significant 24.0% and 18.1% lower than that from Hep G2/pcDNA3 cells, respectively (Fig. 2).

Since ROS formation was decreased in Hep G2/SMP30 cells, we next determined the amount of lipid peroxidation, which was calculated as TBARS products in Hep G2/SMP30 and Hep G2/pcDNA3 cells. TBARS products from Hep G2/SMP30 cells were a significant 43.1% lower than that from Hep G2/pcDNA3 cells (Fig. 3).

Antioxidant Levels in Hep G2/SMP30 Cells To assess whether the over-expression of human SMP30/GNL affects antioxidant levels, we measured the SOD activity and GSH levels in the Hep G2/SMP30 and Hep G2/pcDNA3 cells. Like the decrease in ROS, total SOD activity was also diminished in Hep G2/SMP30 cells, *i.e.*, a significant 42.6% less than in Hep G2/pcDNA3 cells (Fig. 4A). Moreover, the difference was even greater for GSH levels, which in Hep G2/SMP30 cells were a significant 62.4% lower than that in Hep G2/pcDNA3 cells (Fig. 4B). Thus, over-expression of SMP30/GNL in Hep G2 cells contributed to the decrease of ROS formation accompanied by a decrease of lipid peroxidation, *i.e.*, SOD activity and GSH levels.

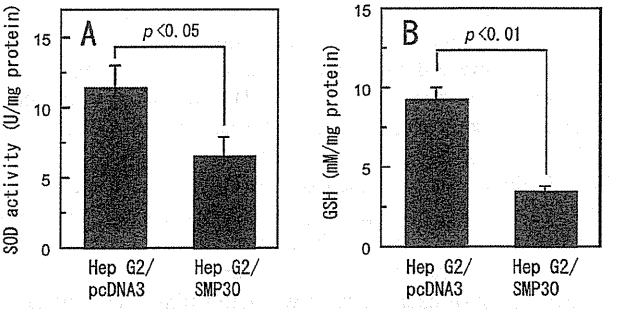

Fig. 4. SOD Activity and GSH Level of the Hep G2/SMP30 and Hep G2/pcDNA3 Mock-Transfected Control Cells

Total SOD activity (A) and GSH level (B) were determined as described in Materials and Methods. Values are expressed as mean±S.D. of five different experiments.

DISCUSSION

We report here, for the first time, that over-expression of SMP30/GNL contributes to the decrease of ROS formation in human hepatic carcinoma Hep G2 cells. Decreased ROS formation resulted in the low levels of lipid peroxidation, SOD activity and GSH we documented in Hep G2/SMP30 cells.

SMP30 was recently identified as a lactone-hydrolyzing enzyme GNL, which is a key enzyme involved in the synthesis of vitamin C in numerous animal species.[10] SMP30/GNL knockout mice developed symptoms of scurvy when fed a vitamin C-deficient diet, verifying the pivotal role of SMP30 in vitamin C biosynthesis. In addition, vitamin C depletion in SMP30/GNL knockout mice resulted in an increase of superoxide generation in the brain.[16,17] Mice, rats and many other animals can synthesize vitamin C *in vivo*; however, humans, monkeys and guinea pigs have lost this ability owing to evolutionary changes that yielded point mutations of the gluconolactone oxidase gene. Logically, then, SMP30/GNL must perform other physiological functions, because SMP30/GNL proteins are produced abundantly in the liver, kidney, pancreas and adrenal cortex of humans.[2] Our previous report described the use of Hep G2/SMP30 cells in which the over-expression of SMP30/GNL resulted in an enhanced Ca^{2+} efflux *via* activation of the calmodulin-dependent Ca^{2+}-pump in Hep G2/SMP30 cells. These cells then became resistant to injury caused by high concentrations of intracellular Ca^{2+}.[18] Furthermore, over-expression of SMP30/GNL in Hep G2 cells induced the formation of numerous microvilli and bile canaliculi.[11] The formation of microvilli and bile canaliculi is essential for the construction of liver tissues and maintenance of liver functions. The association of cytosolic-free Ca^{2+} with cell shape and dynamics of the actin cytoskeleton, as well as the formation and disassembly of cell-to-substrate adhesions, is well known.[19] Ca^{2+} also serves as a second messenger in many biochemical signal-transduction events.[19] These observations strongly suggest that the cause of decreased ROS formation in Hep G2/SMP30 cells may be intracellular Ca^{2+} modulation by SMP30/GNL over-expression.

In addition, we previously examined whether SMP30/GNL has radical scavenging ability by using recombinant human SMP30/GNL, which has enzyme activity and oxidation-sensitive C400 fluorescent dye in the Fe^{2+}/ascorbic acid. This di-

rect system induced ROS generation *in vitro*[20]; however, no radical scavenging ability by SMP30/GNL itself was detected (data not shown). Instead, our present results indicate that the over-expression of SMP30/GNL in Hep G2 cells contributes to a marked decrease of ROS formation as well as a decrease of lipid peroxidation, SOD activity and GSH levels. These results strongly suggest that SMP30/GNL has antioxidant ability indirectly and that the down-regulation of SMP30/GNL during the aging process may increase the formation of ROS to the detriment of cells.

Acknowledgements This study is supported by a Grant-in-Aid for Scientific Research from the Ministry of Education, Science, and Culture, Japan (to S.H. and A.I.), and a Grant-in-Aid for Smoking Research Foundation, Japan (to A.I.). We thank Ms. P. Minick for the excellent editorial assistance.

REFERENCES

1) Fujita T., Uchida K., Maruyama N., *Biochim. Biophys. Acta*, **1116**, 122—128 (1992).
2) Ishigami A., Maruyama N., *Geriatr. Gerontol. Int.*, **7**, 316—325 (2007).
3) Fujita T., Shirasawa T., Uchida K., Maruyama N., *Biochim. Biophys. Acta*, **1132**, 297—305 (1992).
4) Fujita T., Mandel J. L., Shirasawa T., Hino O., Shirai T., Maruyama N., *Biochim. Biophys. Acta*, **1263**, 249—252 (1995).
5) Fujita T., Shirasawa T., Maruyama N., *Biochim. Biophys. Acta*, **1308**, 49—57 (1996).
6) Ishigami A., Handa S., Maruyama N., Supakar P. C., *Biosci. Biotechnol. Biochem.*, **67**, 158—160 (2003).
7) Mori T., Ishigami A., Seyama K., Onai R., Kubo S., Shimizu K., Maruyama N., Fukuchi Y., *Pathol. Int.*, **54**, 167—173 (2004).
8) Ishigami A., Fujita T., Handa S., Shirasawa T., Koseki H., Kitamura T., Enomoto N., Sato N., Shimosawa T., Maruyama N., *Am. J. Pathol.*, **161**, 1273—1281 (2002).
9) Ishigami A., Kondo Y., Nanba R., Ohsawa T., Handa S., Kubo S., Akita M., Maruyama N., *Biochem. Biophys. Res. Commun.*, **315**, 575—580 (2004).
10) Kondo Y., Inai Y., Sato Y., Handa S., Kubo S., Shimokado K., Goto S., Nishikimi M., Maruyama N., Ishigami A., *Proc. Natl. Acad. Sci. U.S.A.*, **103**, 5723—5728 (2006).
11) Ishigami A., Fujita T., Inoue H., Handa S., Kubo S., Kondo Y., Maruyama N., *Cell Tissue Res.*, **320**, 243—249 (2005).
12) Knowles B. B., Howe C. C., Aden D. P., *Science*, **209**, 497—499 (1980).
13) Laemmli U. K., *Nature* (London), **227**, 680—685 (1970).
14) Towbin H., Staehelin T., Gordon J., *Proc. Natl. Acad. Sci. U.S.A.*, **76**, 4350—4354 (1979).
15) Ohkawa H., Ohishi N., Yagi K., *Anal. Biochem.*, **95**, 351—358 (1979).
16) Kondo Y., Sasaki T., Sato Y., Amano A., Aizawa S., Iwama M., Handa S., Shimada N., Fukuda M., Akita M., Lee J., Jeong K. S., Maruyama N., Ishigami A., *Biochem. Biophys. Res. Commun.*, **377**, 291—296 (2008).
17) Sato Y., Kajiyama S., Amano A., Kondo Y., Sasaki T., Handa S., Takahashi R., Fukui M., Hasegawa G., Nakamura N., Fujinawa H., Mori T., Ohta M., Obayashi H., Maruyama N., Ishigami A., *Biochem. Biophys. Res. Commun.*, **375**, 346—350 (2008).
18) Fujita T., Inoue H., Kitamura T., Sato N., Shimosawa T., Maruyama N., *Biochem. Biophys. Res. Commun.*, **250**, 374—380 (1998).
19) Sjaastad M. D., Nelson W. J., *Bioessays*, **19**, 47—55 (1997).
20) Takatsu H., Ogata M., Fukui K., Takeda T., Endo T., Urano S., *Nat. Med.* (Tokyo), **63**, 364—367 (2009).

Circ J 2009; **73:** 2125–2134

Antioxidant, EUK-8, Prevents Murine Dilated Cardiomyopathy

Satoru Kawakami[1,4,5]; Akina Matsuda[1,4]; Tadahiro Sunagawa[1,6]; Yoshihiro Noda[1]; Takao Kaneko[2]; Shoichi Tahara[2]; Yoshimi Hiraumi[7]; Souichi Adachi[7]; Hiromitsu Matsui[8]; Katsuyuki Ando[8]; Toshiro Fujita[8]; Naoki Maruyama[3,4]; Takuji Shirasawa[1,5,9]; Takahiko Shimizu[1,4,5]

Background: Mice lacking manganese-superoxide dismutase (Mn-SOD) activity exhibit the typical pathology of dilated cardiomyopathy (DCM). In the present study, presymptomatic and symptomatic mutant mice were treated with the SOD/catalase mimetic, EUK-8.

Methods and Results: Presymptomatic heart/muscle-specific Mn-SOD-deficient mice (H/M-*Sod2*$^{-/-}$) were treated with EUK-8 ($30\,mg \cdot kg^{-1} \cdot day^{-1}$) for 4 weeks, and then cardiac function and the reactive oxygen species (ROS) production in their heart mitochondria were assessed. EUK-8 treatment suppressed the progression of cardiac dysfunction and diminished ROS production and oxidative damage. Furthermore, EUK-8 treatment effectively reversed the cardiac dilatation and dysfunction observed in symptomatic H/M-*Sod2*$^{-/-}$ mice. Interestingly, EUK-8 treatment repaired a molecular defect in connexin43.

Conclusions: EUK-8 treatment can prevent and cure murine DCM, so SOD/catalase mimetic treatment is proposed as a potential therapy for DCM. (*Circ J* 2009; **73:** 2125–2134)

Key Words: Connexin43 (Cx43); Dilated cardiomyopathy (DCM); EUK-8; Manganese-superoxide dismutase (Mn-SOD); Reactive oxygen species (ROS)

The findings of several clinical studies support the hypothesis that reactive oxygen species (ROS) play an important role in the pathogenesis of cardiovascular diseases such as ischemic heart disease, atherosclerosis, and heart failure.[1] ROS are mainly generated in mitochondria as a byproduct of normal cellular aerobic metabolism. Excess production of ROS, such as superoxide anions (O_2^-) and hydrogen peroxide (H_2O_2), by mitochondria is thought to be associated with increased morbidity. To protect cells from oxidative stress, mammalian cells contain antioxidant molecules, including manganese-superoxide dismutase (Mn-SOD) (in mitochondria), copper/zinc-SOD (in the cytosol), extracellular-SOD (in the extracellular space),[2] glutathione peroxidases, catalase, and other nonenzymatic antioxidants. SOD detoxifies O_2^- radicals via dismutation to produce H_2O_2 and H_2O. Because Mn-SOD is a superoxide scavenger enzyme located in the mitochondrial matrix, it plays a pivotal role in protecting cells from mitochondrial ROS. Two laboratories have independently generated Mn-SOD-deficient mice by deletion of different segments of the *Sod2* gene. These mutant mice suffer neonatal death within 18 days because of dilated cardiomyopathy (DCM), metabolic abnormalities such as ketosis and lactic acidosis, steatosis, and neurodegeneration in the brain, in a strain-dependent manner.[3,4]

Editorial p 2017

In our previous studies, we established several types of tissue-specific Mn-SOD-deficient mice to define the phenotypes observed in systemic Mn-SOD KO mice.[5–7] We reported that heart/muscle-specific Mn-SOD-deficient (H/M-*Sod2*$^{-/-}$) mice showed DCM involving an excess generation of ROS by mitochondria.[6] Moreover, A16V polymorphism of the *Sod2* gene, which is associated with a 30–40% reduction in enzymatic activity, affects idiopathic DCM.[8] These findings suggest that Mn-SOD plays an important role in the susceptibility to DCM onset.

The synthetic salen-manganese complex, EUK-8, possesses both SOD and catalase activity and is a potent SOD/catalase mimetic and antioxidant.[9–11] EUK-8 dismutates O_2^- to H_2O_2 and then further catalyzes its breakdown to O_2 and H_2O. It has been reported that EUK-8 treatment has a protective effects in model organisms associated with ROS-induced pathologies. In vivo studies have shown that EUK-8 improves cardiac mitochondrial dysfunction,[12] delays aging,[13] and prevents adrenergic hypertrophy,[14] ischemia/reperfusion injury,[11] and postischemic reperfusion arrhythmias.[15] Interestingly, EUK-8 treatment extended the lifespan of wild-type nematodes[16] and *Sod2*-null mutant mice.[17] These results suggest that EUK-8 scavenges ROS generated in the cytoplasm or organelles, including mitochondria.

Received March 26, 2009; revised manuscript received July 22, 2009; accepted July 23, 2009; released online September 14, 2009

[1]Molecular Gerontology, [2]Redox Regulation, [3]Aging Regulation, Tokyo Metropolitan Institute of Gerontology, [4]Applied Biological Chemistry, United Graduate School of Agricultural Science, Tokyo University of Agriculture and Technology, [5]Department of Research and Development, Anti-Aging Science, Co Ltd, Tokyo, [6]Research Laboratories for Health & Gustatory Science, Asahi Breweries, Ltd, Ibaraki, [7]Department of Pediatrics, Kyoto University Hospital, Kyoto, [8]Department of Nephrology and Endocrinology, Faculty of Medicine, University of Tokyo and [9]Department of Aging Control Medicine, Juntendo University Graduate School of Medicine, Tokyo, Japan

Mailing address: Takahiko Shimizu, PhD, Molecular Gerontology, Tokyo Metropolitan Institute of Gerontology, 35-2 Sakae-cho, Itabashi-ku, Tokyo 173-0015, Japan. E-mail: shimizut@tmig.or.jp

EUK-8 treatment also reduces ROS generation in heart mitochondria, as well as oxidative DNA and protein damage. Furthermore, EUK-8 dramatically reverses established cardiac dilatation and pump failure. In the present study, we administered EUK-8 to H/M-*Sod2*$^{-/-}$ mice to evaluate its effect on cardiac dilatation and dysfunction. We present the first preclinical data concerning salen-manganese compounds, suggesting the possibility of a new class of drugs for the treatment of DCM.

Methods

Animals

We used H/M-*Sod2*$^{-/-}$ mice, produced by crossbreeding Mn-SOD$^{lox/lox}$ mice with muscle creatine kinase-Cre transgenic mice using in vitro fertilization techniques. Genotyping was performed by tail DNA polymerase chain reaction as described previously.[6] All mice were housed in plastic cages (5 animals/cage) in a pathogen-free barrier facility and were kept under a 12-h light/dark cycle. The mice were maintained and studied according to protocols approved by the Animal Care Committee of the Tokyo Metropolitan Institute of Gerontology.

Isolated Tissue

Images of isolated hearts were obtained with a VHX-100 digital microscope (KEYENCE, Osaka, Japan).

Histological Studies

For histological analysis, heart tissues were immersed in 10% buffered formalin. Fixed tissues were dehydrated, embedded in paraffin, sectioned into 4 μm slices, and stained with hematoxylin–eosin (H&E). Myocardial sections were stained with Azan to evaluate the degree of fibrosis and cardiomyocyte diameter. Images were obtained using a Pixera Pro600EX camera attached to a VANOX-S microscope (Olympus, Tokyo, Japan). The fibrotic area and cardiomyocyte diameter (>30 cells) were quantitatively analyzed with Qwin Plus V3 (Leica Co Ltd). The collagen volume percentage was expressed as the mean of all fields examined for each animal.

Determination of Oxidative DNA Damage

Nuclear DNA was isolated as described previously.[18] Measurement of 8-oxo-2'-deoxyguanosine (8-oxodG) was performed by the electrochemical detection-high-performance liquid chromatography method as described previously.[19] The 8-oxodG content was expressed as the molar ratio of 8-oxodG to 10^6 2'-deoxyguanosine (dG). The amount of dG was calculated from the absorption at 260 nm in the same sample.

Administration of EUK-8

EUK-8 (Calbiochem, San Diego, CA, USA) suspended in saline at 1.5 mg/ml was injected intraperitoneally (30 mg/kg body weight) into the mutant mice once daily.[17] The preventive administration began from 4 weeks of age and continued for 4 weeks. The therapeutic administration began from 16 weeks of age and continued for 2 weeks. Saline was injected as a control.

Echocardiography

The mice were anesthetized with 2.5% avertin (20 μl/g body weight), and echocardiography was performed via ultrasonography (using an EnVisor equipped with a 12-5 MHz Sector transducer; Philips Medical Systems, Andover, MA, USA and an MA or Xario, equipped with a 12-MHz transducer; Toshiba Medical Systems, Tokyo, Japan). The heart was imaged in the 2-dimensional parasternal short-axis view, and an M-mode echocardiogram of the midventricle was recorded at the level of the papillary muscle. Heart rate, anterior and posterior wall thicknesses, and the end-diastolic and systolic internal dimensions of the left ventricle were obtained from the M-mode image.

Measurement of O_2^- and H_2O_2 Production

The mitochondrial fraction was isolated as described previously.[20] O_2^- formation was measured using the chemiluminescent probe 2-methyl-6-*p*-methoxyphenylethynyl-imidazopyazinone (ATTO, Tokyo, Japan).[6] H_2O_2 generation was measured using Amplex Red (Molecular Probes, Eugene, OR, USA).[6,20] Heart mitochondria (4 μg mitochondria protein/well) were incubated with a respiratory substrate (5 mmol/L succinate), 1 μmol/L Amplex Red, 0.2 units/ml horseradish peroxidase, and 0.1% bovine serum albumin. The reactions were performed in triplicate in 100 μl volumes in a 96-well plate. H_2O_2 formation was measured fluorometrically (excitation: 530 nm, emission: 590 nm) over 30 min at 37°C in a SPECTRAmax Gemini XS (Molecular Devices, Sunnyvale, CA, USA). Fluorescence units were converted using the standard curve for a known concentration of H_2O_2. The results are expressed as pmol H_2O_2/μg mitochondria/min.

Measurement of Protein Carbonylation and ATP Content

For the quantitation of cardiac protein carbonylation, the nuclear and mitochondrial fractions of the heart were separated. To prepare the nuclear fractions, crude nuclear fractions were sedimented from tissue homogenates at 1,000 g for 5 min.[20] The nuclear fractions were then washed at 1,000 g for 5 min. The mitochondrial fractions were described before.[20] Nuclear and mitochondrial protein carbonylation was determined by Oxyblot (Chemicon, Billerica, MA, USA) according to the manufacturer's protocol. Immunoreactive spots were visualized with ECL (GE Healthcare, Buckinghamshire, UK) and quantitated using an LAS-3000 (Fujifilm, Tokyo, Japan). ATP content was measured using an ATP measurement kit (TOYO B-Net, Tokyo, Japan) according to the manufacturer's protocol.

Western Blot Analysis

Protein extracts were prepared from heart tissues using extraction buffer composed of 50 mmol/L Tris-HCl (pH 7.4), 150 mmol/L NaCl, 5 mmol/L EDTA, 1% Triton-X 100, and Complete Protease Inhibitor (Roche Diagnostics, Penzberg, Germany). The protein concentration of the samples was measured with a DC protein assay kit (Bio-Rad, Richmond, CA, USA). The proteins were separated by SDS-PAGE, transferred to a PVDF membrane, and detected with specific antibodies for connexin43 (Cx43) (1:1,000; Cell Signaling, Danvers, MA, USA), Mn-SOD (1:10,000; catalog number SOD-111; StressGen, Victoria, Canada), and actin (1:2,500; Sigma, St Louis, MO, USA). The blots were incubated with horseradish peroxidase-conjugated secondary antibodies, and immunoreactive bands were visualized with ECL and LAS-3000.

Statistical Analysis

Data are expressed as means ± SD. Differences among groups

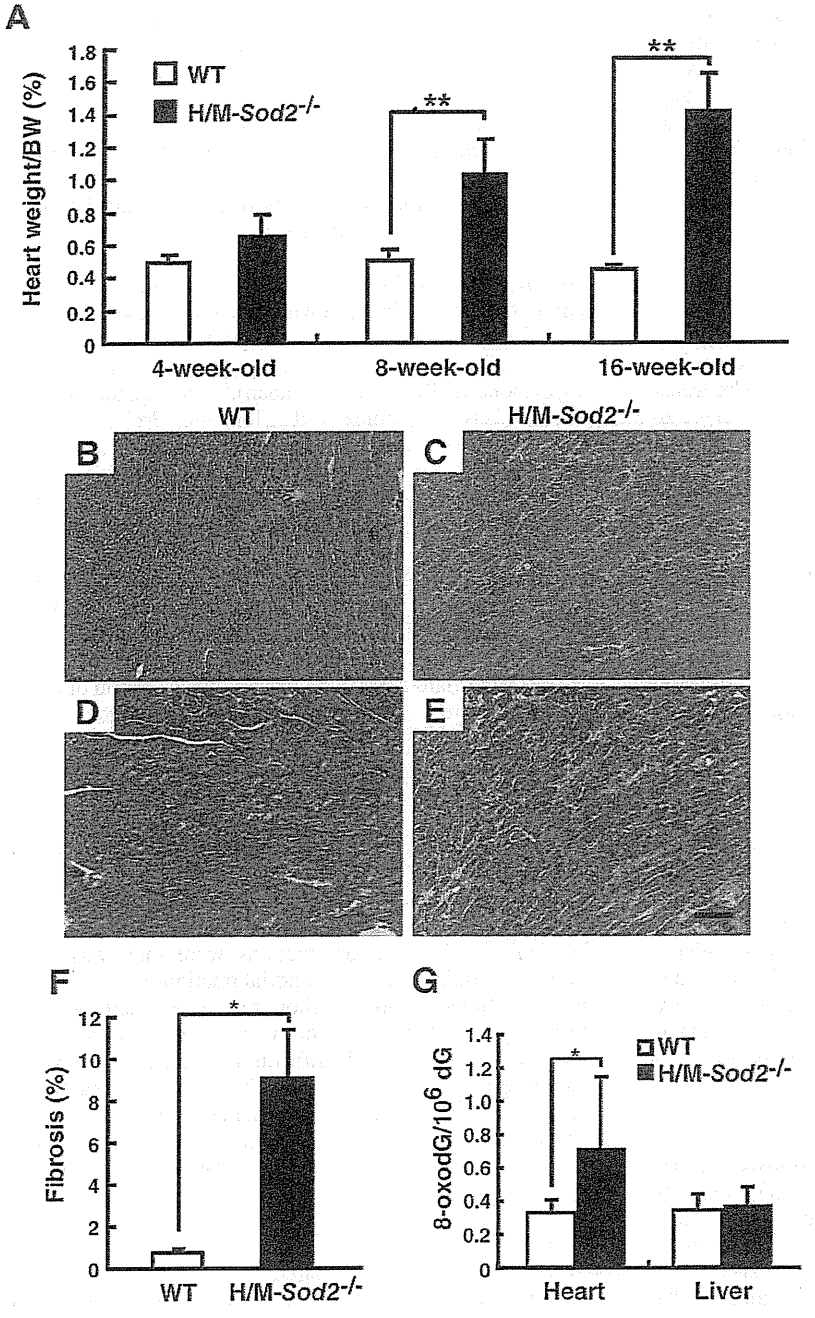

Figure 1. Heart/muscle specific manganese-superoxide dismutase (Mn-SOD) deficiency causes dilated cardiomyopathy in H/M-*Sod2*$^{-/-}$ mice. (**A**) Heart weight to body weight ratios in littermate wild-type (WT) mice (white bars) and H/M-*Sod2*$^{-/-}$ mice (black bars) at 4- (WT: n=3; H/M-*Sod2*$^{-/-}$: n=3), 8- (WT: n=3; H/M-*Sod2*$^{-/-}$: n=14), and 16-weeks of age (WT: n=10; H/M-*Sod2*$^{-/-}$: n=10). Histological samples from WT and H/M-*Sod2*$^{-/-}$ mice (16-week-old) are shown with H&E (**B**,**C**) or Azan staining (**D**,**E**). Scale bar=100 μm. (**F**) Quantified interstitial fibrotic area (%) (WT: n=3; H/M-*Sod2*$^{-/-}$: n=3, 16-week-old). (**G**) Measurement of the ratio of 8-oxodG/10^6 dG in nuclear fractions prepared from 16-week-old WT (white bars, n=8) and H/M–H/M-*Sod2*$^{-/-}$ (black bars, n=8) hearts or livers. 8-oxodG, 8-oxo-2'-deoxyguanosine.

were tested by ANOVA. Comparisons between 2 groups were performed using the paired Student's t-test. $P<0.05$ was considered to be significant.

Results

Mn-SOD Deficiency Causes DCM Associated With Fibrosis

To address the pathological effects of mitochondrial oxidative stress on cardiac function, we generated H/M-*Sod2*$^{-/-}$ mice using a Cre-loxp system. At 4 weeks of age, these mice showed normal heart weights (**Figure 1A**). From 8 weeks of age, however, all H/M-*Sod2*$^{-/-}$ mice showed heart dilatation and progressively increasing heart weight to body weight (HW/BW) ratios (**Figure 1A**). On the other hand, the mice had no obvious abnormalities in their skeletal muscles (data not shown).

In the H/M-*Sod2*$^{-/-}$ mice, H&E staining showed that the left ventricular (LV) wall was characterized by myocardial degeneration, myocyte disarray, and myocardial cells containing irregular myofilaments (**Figures 1B,C**). With Azan staining, there were diffuse fibrotic scars surrounding the myocardial cells (**Figures 1D,E**). Some of the thickened fibrotic foci were caused by myocardial remodeling. Quantitative assessment of the fibrotic area (the ratio of collagen area to total area) showed that the H/M-*Sod2*$^{-/-}$ mice had a 12.3-fold larger fibrotic area compared with age-matched WT mice (**Figure 1F**).

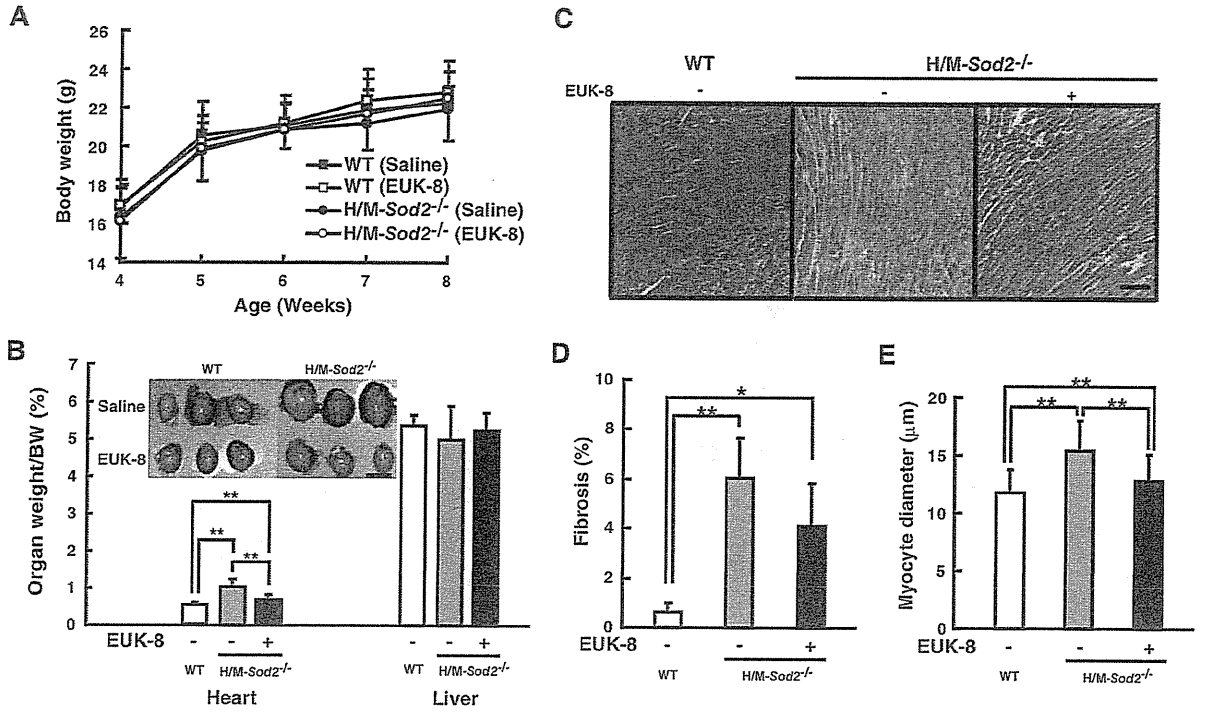

Figure 2. Preventive effects of EUK-8 administration in H/M-*Sod2*$^{-/-}$ mice. The injections began from 4 weeks of age and continued for 4 weeks. (**A**) Body weights of saline-treated wild-type (WT: n=6), EUK-8-treated WT (n=6), saline-treated H/M-*Sod2*$^{-/-}$ mice (n =17), and EUK-8-treated H/M-*Sod2*$^{-/-}$ mice (n=18) during the administration period. (**B**) Representative images of hearts after the treatment period. Normalized heart and liver weights are shown at 8 weeks of age. Representative photomicrographs of mouse heart sections stained with Azan (**C**) and quantification of interstitial fibrosis (**D**) (WT: n=3; saline-treated H/M-*Sod2*$^{-/-}$: n=4; EUK-8-treated H/M-*Sod2*$^{-/-}$: n=4). (**E**) Quantification of cardiomyocyte diameter (WT: n=3; saline-treated H/M-*Sod2*$^{-/-}$: n=4; EUK-8-treated H/M-*Sod2*$^{-/-}$: n=4). *P<0.05, **P<0.01.

To investigate whether Mn-SOD deficiency facilitates oxidative DNA damage in the heart, we next measured the level of 8-oxodG, which is a biomarker of oxidative DNA damage, as quantified by electrochemical detection-HPLC.[19] In heart nuclear DNA, the ratio of 8-oxodG/10^6 dG was increased by 2.2-fold in the H/M-*Sod2*$^{-/-}$ mice compared with that in the wild-type (WT) mice (P<0.05), although there were no differences between the livers of the mutant and WT mice (**Figure 1G**). These results suggest that the accumulation of oxidative damage, such as oxidized DNA, causes DCM in H/M-*Sod2*$^{-/-}$ mice. During aging, the ratio of 8-oxodG/10^6 dG in heart nuclear DNA remained stable from 2 to 24 months, but there was a significant 2-fold increase in the amount of 8-oxodG in the heart nuclear DNA of the C57BL/6 mice and rats >24 months of age.[18,21] Interestingly, the increased amount of 8-oxodG in the nuclear DNA of these aged hearts was similar to that observed in the H/M-*Sod2*$^{-/-}$ mice, suggesting that oxidative stress modifies cardiac nuclear DNA in aged and *Sod2*-deficient mice.

EUK-8 Prevents Cardiac Enlargement in H/M-*Sod2*$^{-/-}$ Mice

It has been reported that the antioxidant EUK-8 significantly extended the lifespan of *sod2* nullzygous mice,[17] and the survival of apoptosis-inducing factor-deficient harlequin mice subjected to pressure overload.[22] EUK-8 also ameliorates the cardiac phenotype of WT mice that have undergone pressure overload.[22] To determine whether treatment with EUK-8 prevents the progression of DCM in H/M-*Sod2*$^{-/-}$ mice, we administered EUK-8 daily, beginning at 4 weeks of age and continuing for 4 weeks. The H/M-*Sod2*$^{-/-}$ and WT mice that were treated with EUK-8 had similar body weight gains to those of the saline-treated groups throughout the experimental period (**Figure 2A**). We found no deleterious effects on growth or general health from the EUK-8 regimen (data not shown). After the administration period, we evaluated the HW/BW ratio, fibrotic area, and cardiomyocyte diameter. Interestingly, EUK-8 treatment prevented macroscopic cardiac enlargement and elevation of the HW/BW ratio in H/M-*Sod2*$^{-/-}$ mice (**Figure 2B**). Azan staining, however, showed that interstitial fibrosis increased by 6.4-fold after EUK-8 treatment, indicating that EUK-8 failed to suppress cardiac fibrosis in the H/M-*Sod2*$^{-/-}$ mice (**Figures 2C,D**). After saline treatment, the fibrotic area increased 9.6-fold in the mutant mice (**Figures 2C,D**). On the other hand, EUK-8 treatment significantly prevented cardiac hypertrophy in the H/M-*Sod2*$^{-/-}$ mice although cardiomyocyte diameter was slightly increased by 1.3-fold in the saline-treated mutant mice compared with WT mice (**Figure 2E**). These findings are significant and indicate that EUK-8 effectively prevented the development of cardiac enlargement, but not fibrosis, in H/M-*Sod2*$^{-/-}$ mice.

To examine whether EUK-8 has any preventive effects on the progression of cardiac dysfunction in H/M-*Sod2*$^{-/-}$ mice, we next performed echocardiographic examinations. Cardiac performance was evaluated at 4 weeks of age (pre-treatment). Despite their normal HW/BW ratio (**Figure 1A**), H/M-*Sod2*$^{-/-}$ mice showed deterioration of echocardiographic parameters, such as the LV end-diastolic internal

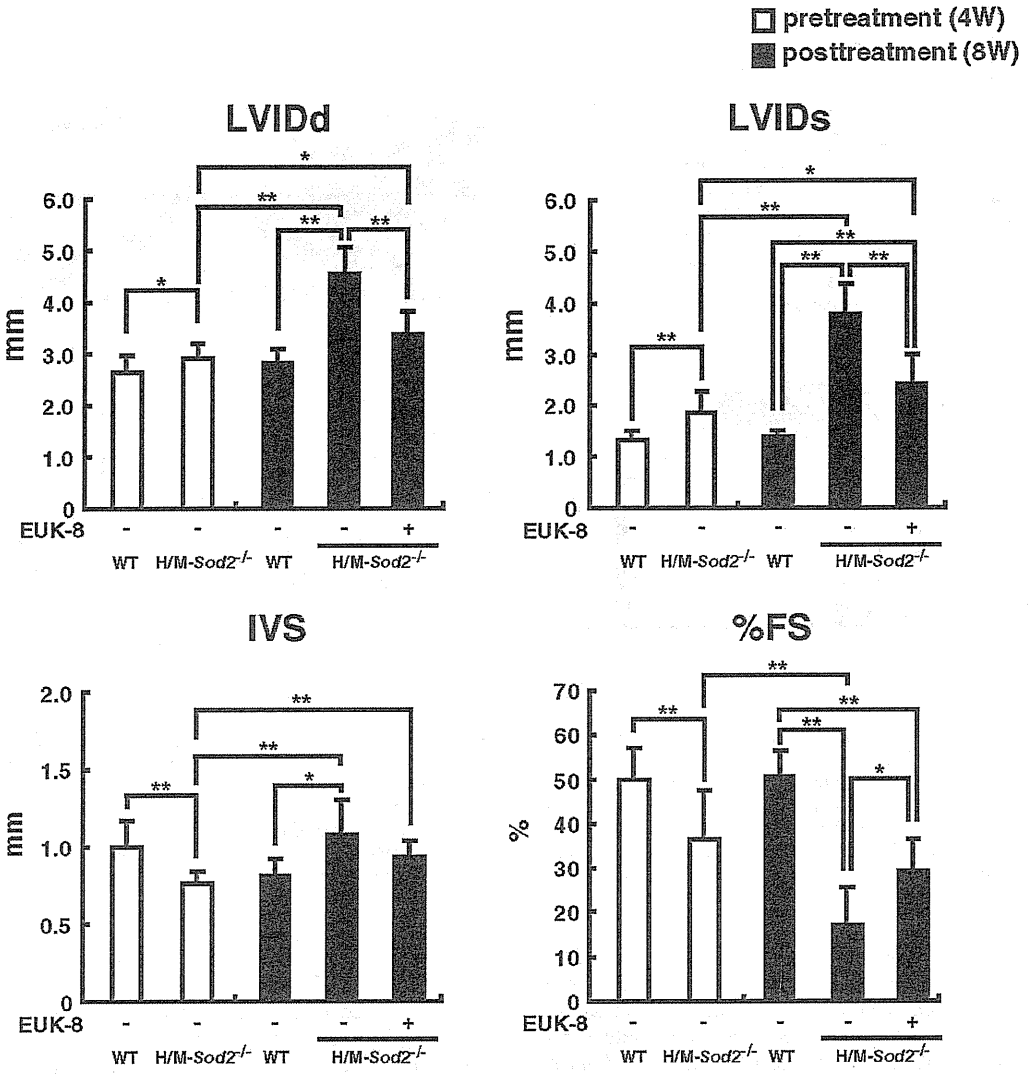

Figure 3. Echocardiographic analysis before and after the treatment period. Echocardiographic parameters include left ventricular end-diastolic internal dimension (LVIDd) and left ventricular end-systolic internal dimension (LVIDs), interventricular septum (IVS), and the percentage of fractional shortening (%FS). (White bars) Pretreatment (WT: n=16, H/M-*Sod2*$^{-/-}$: n=11) at 4 weeks old and (black bars) posttreatment (saline-treated WT: n=6, saline-treated H/M-*Sod2*$^{-/-}$: n=5, EUK-8-treated H/M-*Sod2*$^{-/-}$: n=5) at 8 weeks old. *P<0.05, **P<0.01

dimension (LVIDd), LV end-systolic internal dimension (LVIDs), interventricular septum (IVS), and the percentage of fractional shortening (%FS) (**Figure 3**). At 8 weeks of age, the saline-treated mutant mice had significantly dilated LV internal dimension (P<0.01), thickened IVS (P<0.01), and impaired %FS (P<0.01) (**Figure 3**). After the administration of EUK-8 for 4 weeks, cardiac dilation (LVIDd: P<0.01, LVIDs: P<0.01) and pump failure (%FS: P<0.05) were markedly compared with the saline treatment group (**Figure 3**). These results demonstrate that EUK-8 significantly delays the progression of cardiac dysfunction caused by the loss of Mn-SOD expression.

EUK-8 Reduces ROS Generation and Oxidative Damage

We then examined the generation of O_2^- and H_2O_2, using isolated cardiac mitochondria. When succinate was added as a respiratory substrate, the heart mitochondria in the saline-treated mutant mice generated elevated O_2^- levels (147%, P<0.01) relative to those of the WT mice (P<0.01) (**Figure 4A**). In contrast, EUK-8 treatment significantly decreased O_2^- generation (28%, P<0.05) compared with saline treatment in the mutant mice (**Figure 4A**). H_2O_2 generation in the cardiac mitochondria of the saline-treated mutant mice was reduced by 46% compared with the WT mice (**Figure 4B**), indicating that Mn-SOD deficiency decreases mitochondrial H_2O_2 generation because of a lack of Mn-SOD-mediated dismutation reactions. Furthermore, H_2O_2 generation was also decreased in the EUK-8 treatment group because EUK-8 also possesses catalase activity. Both O_2^- and H_2O_2 generation were decreased in mitochondria isolated from the EUK-8-treated mutant mice.

Because EUK-8 treatment had suppressed excess ROS generation in the cardiac mitochondria of mutant mice, we next analyzed oxidative DNA damage in nuclear DNA isolated from the heart and liver. As shown in **Figure 1G**, there was a 2.2-fold increase in the amount of 8-oxodG

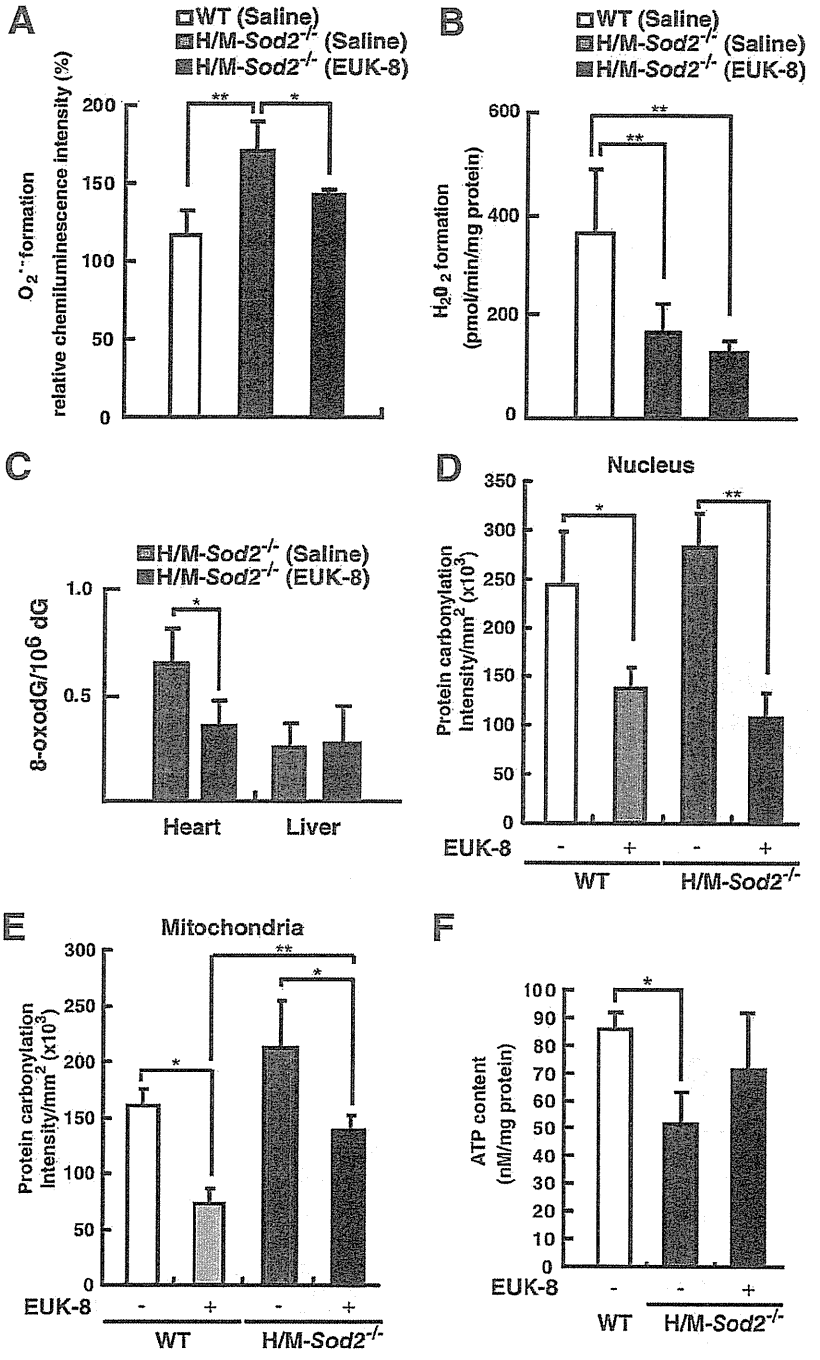

Figure 4. Altered levels of superoxide/hydrogen peroxide and ATP in hearts from H/M-*Sod2*$^{-/-}$ mice treated with EUK-8. (**A**) Mitochondrial superoxide and (**B**) hydrogen peroxide formation in the hearts of saline-treated wild-type (WT) mice (n=5), saline-treated H/M-*Sod2*$^{-/-}$ (n=6), and EUK-8-treated H/M-*Sod2*$^{-/-}$ mice (n=5) at 8 weeks old. (**C**) Measurement of the ratio of 8-oxodG/10^6 dG in nuclear fractions prepared from the heart and liver. The heart nuclei from H/M-*Sod2*$^{-/-}$ mice treated with saline (n=4) showed a higher 8-oxodG level than those from EUK-8-treated H/M-*Sod2*$^{-/-}$ mice at 8 weeks old (n=4). Oxyblot analyses of the nuclear (**D**) and mitochondrial (**E**) fractions isolated from the heart tissue of the saline-treated WT mice (n=3), EUK-8-treated WT mice (n=3), saline-treated H/M-*Sod2*$^{-/-}$ mice (n=3), and EUK-8-treated H/M-*Sod2*$^{-/-}$ mice (n=3) at 8 weeks old. The oxyblot results were quantified by intensity/mm^2. *P<0.05, **P<0.01. (**F**) ATP content in the hearts of saline-treated WT mice (n=4), saline-treated H/M-*Sod2*$^{-/-}$ mice (n=4), and EUK-8-treated H/M-*Sod2*$^{-/-}$ mice at 8 weeks old (n=3). *P<0.05, **P<0.01. 8-oxodG, 8-oxo-2'-deoxyguanosine.

in the nuclear DNA of the H/M-*Sod2*$^{-/-}$ mice. As expected, EUK-8 treatment caused a 2-fold decrease in the ratio of 8-oxodG/10^{6}dG in the heart nuclear DNA (P<0.05) of the H/M-*Sod2*$^{-/-}$ mice (**Figure 4C**), but did not affect the nuclear DNA in the liver (**Figure 4C**). Next, to investigate oxidative protein damage in nuclei and mitochondria, we analyzed the protein carbonylation of fractionated nuclear and mitochondrial proteins in the H/M-*Sod2*$^{-/-}$ mice. Protein carbonylation was elevated in the nuclear and mitochondrial fractions, but the difference was not statistically significant (**Figures 4D,E**). EUK-8 treatment significantly reduced both nuclear and mitochondrial protein carbonylation in H/M-*Sod2*$^{-/-}$ mice (**Figures 4D,E**). Interestingly, EUK-8 also decreased the expression of oxidative proteins in both fractions in the WT mice (**Figures 4D,E**). These results indicate that excess ROS generation, as well as oxidative DNA and protein damage, are significantly suppressed by EUK-8.

It has been reported that the ATP content of failing human hearts is 25–30% lower than that of healthy hearts.[23,24] Moreover, we have previously reported that the ATP content in H/M-*Sod2*$^{-/-}$ hearts is approximately 50% lower than that of control mice.[6] Because EUK-8 treatment improved cardiac contractility in mutant mice (**Figure 3**), we examined the heart's ATP content. In the hearts of mutants that

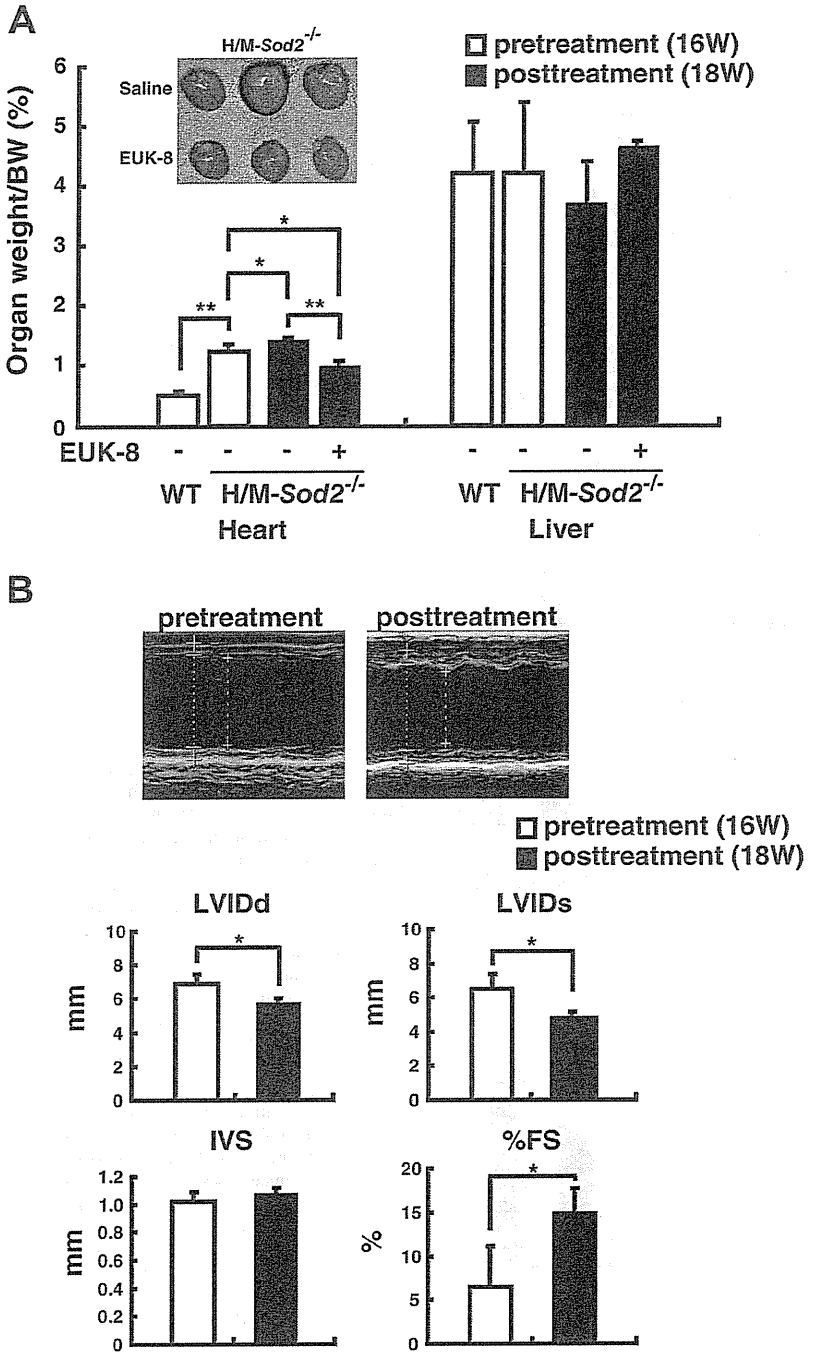

Figure 5. Therapeutic effects of EUK-8 administration to H/M-*Sod2*$^{-/-}$ mice associated with serious cardiac morbidity. Injections began from 16 weeks old and continued for 2 weeks. (**A**) Representative images of hearts taken after the treatment period. Normalized weights of organs pretreatment (WT mice: n=11, H/M-*Sod2*$^{-/-}$ mice: n=6) at 16 weeks old and post-treatment (saline-treated H/M-*Sod2*$^{-/-}$: n=3, EUK-8-treated H/M-*Sod2*$^{-/-}$ mice: n=3) at 18 weeks old. (**B**) Transthoracic M-mode echocardiographic tracings from before (**Left**) and after (**Right**) EUK-8 administration period (**Top**). (**Bottom**) Echocardiographic parameters pre-treatment (H/M-*Sod2*$^{-/-}$: n=4) at 16 weeks old and post-EUK-8 treatment (H/M-*Sod2*$^{-/-}$: n=4) at 18 weeks old. LVIDd, left ventricular end-diastolic internal dimension; LVIDs, left ventricular end-systolic internal dimension; IVS, interventricular septum; %FS, percentage of fractional shortening. *P<0.05, **P<0.01.

had been treated with saline it was significantly decreased to 39.9% of the level in the WT mice. In contrast, EUK-8 treatment recovered 22.7% more ATP content than did saline treatment in the mutant mice, but the difference was not statistically significant (**Figure 4D**).

EUK-8 Reverses Cardiac Enlargement and Dysfunction in H/M-*Sod2*$^{-/-}$ Mice

To examine the potential of EUK-8 as a therapeutic agent for DCM, we analyzed whether EUK-8 treatment was able to reverse established DCM in 16-week-old H/M-*Sod2*$^{-/-}$ mice. As previously described, the HW/BW ratio and cardiac contractility of 16-week-old H/M-*Sod2*$^{-/-}$ mice were significantly exacerbated.[6] Interestingly, after administration of EUK-8 for 2 weeks, cardiac dilatation was dramatically improved in the H/M-*Sod2*$^{-/-}$ mice compared with saline-treated mutant mice, and EUK-8 also significantly ameliorated the HW/BW ratio compared with pretreatment and after saline treatment (**Figure 5A**). In the echocardiographic analysis, cardiac dilation (LVIDd: P<0.05, LVIDs: P<0.05) and contractility (%FS: P<0.05) were also improved by administration of EUK-8 compared with their pretreatment levels in mutant mice (**Figure 5B**). These results indicate that EUK-8 dramatically reversed established DCM caused

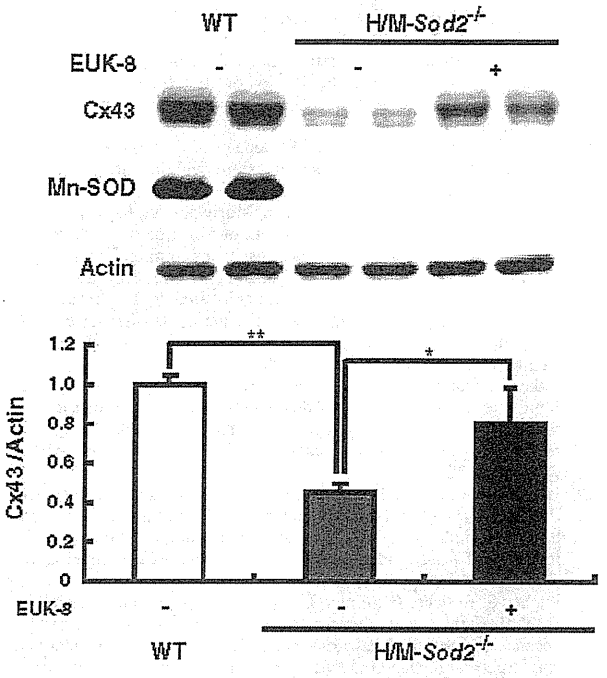

Figure 6. Gap junction protein, connexin 43 (Cx43), is degraded in H/M-*Sod2*$^{-/-}$ hearts. (**Top**) Western blot analysis of proteins extracted from the hearts of saline-treated wild-type (WT), H/M-*Sod2*$^{-/-}$, and EUK-8-treated H/M-*Sod2*$^{-/-}$ mice using antibodies against Cx43, manganese-superoxide dismutase (Mn-SOD), and actin. (**Bottom**) Western blot results for Cx43 were quantified by densitometry and the level was normalized to that of actin (n=5). *P<0.05, **P<0.01.

by mitochondrial oxidative stress related to Mn-SOD deficiency.

EUK-8 Recovers Cx43 Expression in H/M-*Sod2*$^{-/-}$ Mice

In preliminary experiments, we detected a drastic downregulation of Cx43 in the hearts of H/M-*Sod2*$^{-/-}$ mice. Cx43 is a major gap junction protein that regulates cardiac conduction.[25,26] It is speculated that Cx43 downregulation causes the development or progression of heart failure in H/M-*Sod2*$^{-/-}$ mice, so to test this, we investigated levels of Cx43 in H/M-*Sod2*$^{-/-}$ mice. As shown in **Figure 6**, the levels of Cx43 were markedly reduced in the hearts of saline-treated H/M-*Sod2*$^{-/-}$ mice (P<0.01). Interestingly, EUK-8 treatment significantly improved the Cx43 levels compared with saline-treatment (P<0.05), which indicates that EUK-8 treatment restores the downregulated expression of Cx43 or suppresses the enhanced degradation of Cx43. Microarray analysis showed that Cx43 expression was altered by Mn-SOD deficiency (0.50-fold, compared with WT mice). However, no obvious change was observed in Cx43 expression after EUK-8 treatment (0.60-fold, compared with WT mice). Therefore, the results of the immunoblot analysis suggest that EUK-8 treatment suppressed the enhanced degradation of Cx43 in the hearts of mutant mice (**Figure 6**).

Discussion

In the present study, we have shown that the synthetic antioxidant EUK-8 prevents cardiac enlargement and dysfunction in H/M-*Sod2*$^{-/-}$ mice (**Figures 2,3**). Our findings suggest that the class of synthetic catalytic "mitoprotective" antioxidants exemplified by EUK-8 can permeate through the plasma membrane of cardiomyocytes, gain access to mitochondria, and attenuate excess ROS generation. These protective effects of EUK-8 lead to the suppression of oxidative DNA and mitochondrial protein damage (**Figures 4C, E**). EUK-8 treatment also restored the cardiac ATP level, as well as cardiac contractility, and induced improvements in LV dilation and heart weight. Melov et al reported that EUK-8 prevented the loss of mitochondrial aconitase activity in the brains of *Sod2*-null mice,[17] and restored decreased mitochondrial succinate dehydrogenase activity in the hearts of *Sod2*-null mice via its antioxidant effect.[11,12,22] Those reports suggest that EUK-8 protects mitochondrial enzymes involved in the Krebs cycle and respiratory chain, indicating that it improves mitochondrial function via mitoprotective effects. Taken together, the results suggest that attenuation of oxidative damage improves impaired cardiac function in H/M-*Sod2*$^{-/-}$ mice.

ROS are associated with a wide range of age-related disorders, including Alzheimer's disease, Parkinson's disease, myocardial arrhythmias, and heart failure.[1,27,28] These disorders commonly show increased levels of 8-oxodG in serum.[29] Kono et al reported that the levels of 8-oxodG were elevated in the serum and myocardium of patients with DCM.[30] In the present study, we showed a 2.2-fold increase in 8-oxodG in the cardiac nuclear DNA of H/M-*Sod2*$^{-/-}$ mice (**Figure 1G**), and EUK-8 treatment significantly suppressed 8-oxodG formation in nuclear DNA (**Figure 4C**). Although we failed to show the molecular mechanisms through which mitochondrial Mn-SOD-deficiency causes the oxidation of nuclear DNA, we speculate that peroxynitrite mediates oxidative modification of nuclear DNA. O_2^- leakage from mutant mitochondria might induce the formation of cytoplasmic peroxynitrite via a reaction with cellular nitric oxide (NO). In our microarray analysis, we showed that neuronal NO synthase (nNOS) was upregulated by 9.1-fold in the hearts of the H/M-*Sod2*$^{-/-}$ mice (data not shown), suggesting that increased nNOS enhances NO production in the cardiomyocytes of these mice. Analysis of cardiac NO and peroxynitrite levels could shed light on the molecular mechanisms of oxidative modification in nuclear DNA and proteins in H/M-*Sod2*$^{-/-}$ mice. Although we did not measure the level of mitochondrial 8-oxodG, we showed that EUK-8 treatment reduced the level of mitochondrial protein carbonylation in the hearts of H/M-*Sod2*$^{-/-}$ mice (**Figure 4F**). These results permit us to speculate that EUK-8 treatment also suppresses oxidative mitochondrial DNA damage.

Digitalis, β-blockers, angiotensin-converting enzyme inhibitors, and diuretic drugs are the currently used therapeutic agents for DCM. The β-blocker, carvedilol, reduces the morbidity and mortality of patients with congestive heart failure,[31] and more importantly, carvedilol and several of its metabolites possess potent antioxidant activity.[32] We examined whether other antioxidants, MnTBAP[6] and CoQ_{10} (data not shown), would improve the symptoms of H/M-*Sod2*$^{-/-}$ mice and found that their protective or therapeutic effects were weaker than those of EUK-8, a result that implies antioxidant therapy may be effective for the treatment of DCM, particularly EUK-8. On the other hand, we can not exclude the possibility that the observed protective effects of EUK-8 in the hearts of the H/M-*Sod2*$^{-/-}$ mice might have been caused by factors other than its antioxidant capability. Barandier et al reported that EUK-8 has significant vasodilatory effects.[33] EUK-8 might maintain LV func-

tion in H/M-*Sod2*$^{-/-}$ mice through vasodilatory rather than antioxidant activity. Further studies are needed to clarify the protective effects of EUK-8 in vivo.

During histochemical analysis, we found no reduction in fibrosis after EUK-8 treatment in the H/M-*Sod2*$^{-/-}$ mice (**Figure 2D**), whereas van Empel et al reported that EUK-8 treatment significantly reduced cardiac fibrosis in harlequin mice.[22] The differences in the preventive effects of EUK-8 on fibrogenesis are still unexplained. One possibility is that the cardiac fibrosis caused by Mn-SOD deficiency is not the same as that caused by pressure overload. Another possibility is that the antioxidant effects of EUK-8 might be limited to fibrogenesis induced by Mn-SOD deficiency.

Connexins are transmembrane proteins, the best known function of which is to form gap junction channels.[25,26,34] In human studies, downregulation of the principal gap junction protein, Cx43, was implicated in arrhythmia in ischemic heart disease and heart failure caused by DCM.[25,35] In this study, we showed that Cx43 was downregulated in H/M-*Sod2*$^{-/-}$ hearts and when EUK-8 was administered to the mutant mice, the Cx43 level significantly improved without transcriptional restoration. These results suggest that EUK-8 protects against the downregulation of Cx43 caused by posttranslational mechanisms such as degradation and modification. Several studies have focused on oxidative stress and protein downregulation. Mitochondrial aconitase and succinate dehydrogenase activity were found to be reduced in Mn-SOD-deficient mice.[3] Moreover, the IRP1 and ApoB proteins are also downregulated in the livers of CuZn-SOD-deficient mice.[36,37] Excess ROS present during SOD-deficiency may attack specific target molecules in cells, leading to the degradation of proteins. Our data suggest that Cx43 is a target molecule of mitochondrial ROS in the heart.

In conclusion, we demonstrated the efficacy and limitations of the antioxidant EUK-8 in murine DCM. We also indicate the possibility that antioxidants are powerful tools for preventing age-related and/or oxidative stress-dependent heart diseases. Further studies with our model mice will provide opportunities to develop novel medicines for the treatment of heart diseases.

Acknowledgments

We thank Y. Ozawa, E. Moriizumi, Y. Ikeda, T. Horie, M. Takahashi, K. Murakami, M. Ogawara, Y. Kondo, J. Inagaki, T. Tsuda, and H. Okuda (Tokyo Metropolitan Institute of Gerontology) for their valuable discussion and technical support. We also thank Drs M. Tagashira and T. Kanda (Research Laboratories for Health & Gustatory Science, Asahi Breweries, Ltd) for their technical support.

This work was supported by the Program for the Promotion of Basic Research Activities for Innovative Biosciences (T. Shimizu) and by Grants-in-Aid for Scientific Research (B) (Nos. 17390085 and 20390085 to T. Shirasawa), (C) (No. 20500641 to T. Shimizu) and Young Scientists (B) (No. 17790201 to T. Shimizu) from the Ministry of Education, Culture, Sports, Science and Technology.

References

1. Giordano FJ. Oxygen, oxidative stress, hypoxia, and heart failure. *J Clin Invest* 2005; **115:** 500–508.
2. Maier CM, Chan PH. Role of superoxide dismutases in oxidative damage and neurodegenerative disorders. *Neuroscientist* 2002; **8:** 323–334.
3. Li Y, Huang TT, Carlson EJ, Melov S, Ursell PC, Olson JL, et al. Dilated cardiomyopathy and neonatal lethality in mutant mice lacking manganese superoxide dismutase. *Nat Genet* 1995; **11:** 376–381.
4. Lebovitz RM, Zhang H, Vogel H, Cartwright J Jr, Dionne L, Lu N, et al. Neurodegeneration, myocardial injury, and perinatal death in mitochondrial superoxide dismutase-deficient mice. *Proc Natl Acad Sci USA* 1996; **93:** 9782–9787.
5. Ikegami T, Suzuki Y, Shimizu T, Isono K, Koseki H, Shirasawa T. Model mice for tissue-specific deletion of the manganese superoxide dismutase (MnSOD) gene. *Biochem Biophys Res Commun* 2002; **296:** 729–736.
6. Nojiri H, Shimizu T, Funakoshi M, Yamaguchi O, Zhou H, Kawakami S, et al. Oxidative stress causes heart failure with impaired mitochondrial respiration. *J Biol Chem* 2006; **281:** 33789–33801.
7. Misawa H, Nakata K, Matsuura J, Moriwaki Y, Kawashima K, Shimizu T, et al. Conditional knockout of Mn superoxide dismutase in postnatal motor neurons reveals resistance to mitochondrial generated superoxide radicals. *Neurobiol Dis* 2006; **23:** 169–177.
8. Valenti L, Conte D, Piperno A, Dongiovanni P, Fracanzani AL, Fraquelli M, et al. The mitochondrial superoxide dismutase A16V polymorphism in the cardiomyopathy associated with hereditary haemochromatosis. *J Med Genet* 2004; **41:** 946–950.
9. Baker K, Marcus CB, Huffman K, Kruk H, Malfroy B, Doctrow SR. Synthetic combined superoxide dismutase/catalase mimetics are protective as a delayed treatment in a rat stroke model: A key role for reactive oxygen species in ischemic brain injury. *J Pharmacol Exp Ther* 1998; **284:** 215–221.
10. van Empel VP, Bertrand AT, van der Nagel R, Kostin S, Doevendans PA, Crijns HJ, et al. Downregulation of apoptosis-inducing factor in harlequin mutant mice sensitizes the myocardium to oxidative stress-related cell death and pressure overload-induced decompensation. *Circ Res* 2005; **96:** e92–e101.
11. Pucheu S, Boucher F, Sulpice T, Tresallet N, Bonhomme Y, Malfroy B, et al. EUK-8, a synthetic catalytic scavenger of reactive oxygen species, protects isolated iron-overloaded rat heart from functional and structural damage induced by ischemia/reperfusion. *Cardiovasc Drugs Ther* 1996; **10:** 331–339.
12. Morten KJ, Ackrell BA, Melov S. Mitochondrial reactive oxygen species in mice lacking superoxide dismutase 2: Attenuation via antioxidant treatment. *J Biol Chem* 2006; **281:** 3354–3359.
13. Xu Y, Armstrong SJ, Arenas IA, Pehowich DJ, Davidge ST. Cardioprotection by chronic estrogen or superoxide dismutase mimetic treatment in the aged female rat. *Am J Physiol Heart Circ Physiol* 2004; **287:** H165–H171.
14. Amin JK, Xiao L, Pimental DR, Pagano PJ, Singh K, Sawyer DB, et al. Reactive oxygen species mediate alpha-adrenergic receptor-stimulated hypertrophy in adult rat ventricular myocytes. *J Mol Cell Cardiol* 2001; **33:** 131–139.
15. Tanguy S, Boucher FR, Malfroy B, de Leiris JG. Free radicals in reperfusion-induced arrhythmias: Study with EUK 8, a novel non-protein catalytic antioxidant. *Free Radic Biol Med* 1996; **21:** 945–954.
16. Melov S, Ravenscroft J, Malik S, Gill MS, Walker DW, Clayton PE, et al. Extension of life-span with superoxide dismutase/catalase mimetics. *Science* 2000; **289:** 1567–1569.
17. Melov S, Doctrow SR, Schneider JA, Haberson J, Patel M, Coskun PE, et al. Lifespan extension and rescue of spongiform encephalopathy in superoxide dismutase 2 nullizygous mice treated with superoxide dismutase-catalase mimetics. *J Neurosci* 2001; **21:** 8348–8353.
18. Kaneko T, Tahara S, Matsuo M. Non-linear accumulation of 8-hydroxy-2'-deoxyguanosine, a marker of oxidized DNA damage, during aging. *Mutat Res* 1996; **316:** 277–285.
19. Kaneko T, Tahara S, Takabayashi F, Harada N. Suppression of 8-oxo-2'-deoxyguanosine formation and carcinogenesis induced by N-nitrosobis (2-oxopropyl)amine in hamsters by esculetin and esculin. *Free Radic Res* 2004; **38:** 839–846.
20. Van Remmen H, Williams MD, Guo Z, Estlack L, Yang H, Carlson EJ, et al. Knockout mice heterozygous for Sod2 show alterations in cardiac mitochondrial function and apoptosis. *Am J Physiol Heart Circ Physiol* 2001; **281:** H1422–H1432.
21. Hamilton ML, Van Remmen H, Drake JA, Yang H, Guo ZM, Kewitt K, et al. Does oxidative damage to DNA increase with age? *Proc Natl Acad Sci USA* 2001; **98:** 10469–10474.
22. van Empel VP, Bertrand AT, van Oort RJ, van der Nagel R, Engelen M, van Rijen HV, et al. EUK-8, a superoxide dismutase and catalase mimetic, reduces cardiac oxidative stress and ameliorates pressure overload-induced heart failure in the harlequin mouse mutant. *J Am Coll Cardiol* 2006; **48:** 824–832.
23. Nascimben L, Ingwall JS, Pauletto P, Friedrich J, Gwathmey JK, Saks V, et al. Creatine kinase system in failing and nonfailing human myocardium. *Circulation* 1996; **94:** 1894–1901.
24. Starling RC, Hammer DF, Altschuld RA. Human myocardial ATP content and in vivo contractile function. *Mol Cell Biochem* 1998; **180:** 171–177.
25. Severs NJ, Coppen SR, Dupont E, Yeh HI, Ko YS, Matsushita T.

Gap junction alterations in human cardiac disease. *Cardiovasc Res* 2004; **62:** 368–377.
26. Sasano C, Honjo H, Takagishi Y, Uzzaman M, Emdad L, Shimizu A, et al. Internalization and dephosphorylation of connexin43 in hypertrophied right ventricles of rats with pulmonary hypertension. *Circ J* 2007; **71:** 382–389.
27. Klein JA, Ackerman SL. Oxidative stress, cell cycle, and neurodegeneration. *J Clin Invest* 2003; **111:** 785–793.
28. Ide T, Tsutsui H, Kinugawa S, Suematsu N, Hayashidani S, Ichikawa K, et al. Direct evidence for increased hydroxyl radicals originating from superoxide in the failing myocardium. *Circ Res* 2000; **86:** 152–157.
29. Keith M, Geranmayegan A, Sole MJ, Kurian R, Robinson A, Omran AS, et al. Increased oxidative stress in patients with congestive heart failure. *J Am Coll Cardiol* 1998; **31:** 1352–1356.
30. Kono Y, Nakamura K, Kimura H, Nishii N, Watanabe A, Banba K, et al. Elevated levels of oxidative DNA damage in serum and myocardium of patients with heart failure. *Circ J* 2006; **70:** 1001–1005.
31. Packer M, Bristow MR, Cohn JN, Colucci WS, Fowler MB, Gilbert EM, et al. The effect of carvedilol on morbidity and mortality in patients with chronic heart failure: US Carvedilol Heart Failure Study Group. *N Engl J Med* 1996; **334:** 1349–1355.
32. Yue TL, Cheng HY, Lysko PG, McKenna PJ, Feuerstein R, Gu JL, et al. Carvedilol, a new vasodilator and beta adrenoceptor antagonist, is an antioxidant and free radical scavenger. *J Pharmacol Exp Ther* 1992; **263:** 92–98.
33. Barandier C, Boucher F, Malfroy B, de Leiris J. Vasodilatory effects of a salen-manganese complex with potent oxyradical scavenger activities. *J Vasc Res* 1997; **34:** 49–57.
34. Yip HK, Chang LT, Wu CJ, Sheu JJ, Youssef AA, Pei SN, et al. Autologous bone marrow-derived mononuclear cell therapy prevents the damage of viable myocardium and improves rat heart function following acute anterior myocardial infarction. *Circ J* 2008; **72:** 1336–1345.
35. Chen X, Zhang Y. Myocardial Cx43 expression in the cases of sudden death due to dilated cardiomyopathy. *Forensic Sci Int* 2006; **162:** 170–173.
36. Starzynski RR, Lipinski P, Drapier JC, Diet A, Smuda E, Bartlomiejczyk T, et al. Down-regulation of iron regulatory protein 1 activities and expression in superoxide dismutase 1 knock-out mice is not associated with alterations in iron metabolism. *J Biol Chem* 2005; **280:** 4207–4212.
37. Uchiyama S, Shimizu T, Shirasawa T. CuZn-SOD deficiency causes ApoB degradation and induces hepatic lipid accumulation by impaired lipoprotein secretion in mice. *J Biol Chem* 2006; **281:** 31713–31719.

Endocrinology. First published ahead of print November 24, 2009 as doi:10.1210/en.2009-1163

Senescence Marker Protein-30/Gluconolactonase Deletion Worsens Glucose Tolerance through Impairment of Acute Insulin Secretion

Goji Hasegawa, Masahiro Yamasaki, Mayuko Kadono, Muhei Tanaka, Mai Asano, Takafumi Senmaru, Yoshitaka Kondo, Michiaki Fukui, Hiroshi Obayashi, Naoki Maruyama, Naoto Nakamura, and Akihito Ishigami

Department of Endocrinology and Metabolism (G.H., M.Y., M.K., M.T., M.A., T.S., M.F., N.N.), Kyoto Prefectural University of Medicine Graduate School of Medical Science, Kyoto 602-8556, Japan; Aging Regulation (Y.K., N.M.), Tokyo Metropolitan Institute of Gerontology, Tokyo 173-0015, Japan; Institute of Bio-Response Informatics (H.O.), Kyoto 612-8016, Japan; and Department of Biochemistry (A.I.), Faculty of Pharmaceutical Sciences, Toho University, Chiba 274-8510, Japan

Senescence marker protein-30 (SMP30) is an androgen-independent factor that decreases with age. We recently identified SMP30 as the lactone-hydrolyzing enzyme gluconolactonase (GNL), which is involved in vitamin C biosynthesis in animal species. To examine whether the age-related decrease in SMP30/GNL has effects on glucose homeostasis, we used SMP30/GNL knockout (KO) mice treated with L-ascorbic acid. In an ip glucose tolerance test at 15 wk of age, blood glucose levels in SMP30/GNL KO mice were significantly increased by 25% at 30 min after glucose administration compared with wild-type (WT) mice. Insulin levels in SMP30/GNL KO mice were significantly decreased by 37% at 30 min after glucose compared with WT mice. Interestingly, an insulin tolerance test showed a greater glucose-lowering effect in SMP30/GNL KO mice. High-fat diet feeding severely worsened glucose tolerance in both WT and SMP30/GNL KO mice. Morphometric analysis revealed no differences in the degree of high-fat diet-induced compensatory increase in β-cell mass and proliferation. In the static incubation study of islets, insulin secretion in response to 20 mM glucose or KCl was significantly decreased in SMP30/GNL KO mice. On the other hand, islet ATP content at 20 mM in SMP30/GNL KO mice was similar to that in WT mice. Collectively, these data indicate that impairment of the early phase of insulin secretion due to dysfunction of the distal portion of the secretion pathway underlies glucose intolerance in SMP30/GNL KO mice. Decreased SMP30/GNL may contribute to the worsening of glucose tolerance that occurs in normal aging. (*Endocrinology* **151: 0000–0000, 2010**)

Senescence marker protein-30 (SMP30), a 34-kDa protein originally identified in rat liver, is a novel molecule whose expression decreases with age in a sex-independent manner (1, 2). SMP30 transcripts have been detected in multiple tissues, and its amino acid alignment reveals a highly conserved structure among humans, rats, and mice (2). We previously reported that SMP30 participates in Ca^{2+} efflux by activating the calmodulin-dependent Ca^{2+} pump in HepG2 cells and renal tubular cells, conferring on these cells a resistance to injury caused by high intracellular Ca^{2+} concentrations (3, 4). Recently, we identified SMP30 as glucolactonase (GNL), which is involved in L-ascorbic acid biosynthesis in mammals, although human beings are unable to synthesize vitamin C *in vivo* because there are many mutations in their gulonolactone oxidase gene, which catalyzes the conversion of L-gulono-γ-lactone to L-ascorbic acid (5).

To clarify the causal relationship between decreased SMP30/GNL and age-associated physiological changes, we created SMP30/GNL knockout (KO) mice (6). The

ISSN Print 0013-7227 ISSN Online 1945-7170
Printed in U.S.A.

doi: 10.1210/en.2009-1163 Received October 1, 2009. Accepted October 26, 2009.

Abbreviations: AUC, Area under the curve; BrdU, 5-bromo-2-deoxyuridine; GNL, gluconolactonase; HFD, high-fat diet; KO, knockout; NEFA, nonesterified fatty acid; SD, standard diet; SMP30, senescence marker protein-30; WT, wild-type.

livers of SMP30/GNL KO mice were highly susceptible to TNFα- and Fas-mediated apoptosis (6). In addition, their livers showed abnormal accumulation of triglycerides, cholesterol, and phospholipids (7). The lungs of SMP30/GNL KO mice developed alveolar air sac enlargement similar to the senile lung syndrome seen in some elderly people (8, 9). The deposition of lipofuscin, an aging marker, was observed in renal tubular epithelial cells in these mice (2). Furthermore, SMP30/GNL in the brain and lungs has been proposed to have protective effects against oxidative stress associated with aging (9, 10). Although the physiological function of SMP30/GNL is still not entirely clear, our studies using SMP30/GNL KO mice have revealed that a reduction in SMP30/GNL expression may account for the age-associated deterioration of cellular function and the enhanced susceptibility to harmful stimuli in aged tissue. Also, these mice displayed symptoms of scurvy when fed a vitamin C-deficient diet (5, 11–13).

The reduction of carbohydrate metabolism in the elderly is one of the hallmarks of the aging process, and substantial evidence shows that increasing age is associated with worsened glucose tolerance and type 2 diabetes (14, 15). However, the molecular abnormalities that occur in the elderly have not been fully elucidated. Because SMP30/GNL KO mice show phenotypic changes that mimic the premature aging process, we hypothesized that a reduction in SMP30/GNL expression could be linked to the worsening of glucose tolerance that occurs with normal aging. The purpose of this study was to examine the role of SMP30/GNL in glucose homeostasis using SMP30/GNL KO mice.

Materials and Methods

Animals

SMP30/GNL KO mice were generated as described earlier by gene targeting in the background strain C57BL/6 (6). All studies were performed on male mice using age-matched, wild-type (WT) male C57BL/6CrSlc mice (Shimizu Laboratory Supplies Co., Ltd., Kyoto, Japan) as controls. Mice were fed a high-fat diet (HFD 32; 507.6 kcal/100 g, fat kcal 56.7%; CLEA Japan, Tokyo, Japan) or a standard diet (SD; 346.8 kcal/100 g, fat kcal 10%, CLEA Japan) for 8 wk from 7 wk of age. As we have previously reported, SMP30/GNL KO mice cannot synthesize vitamin C *in vivo* because SMP30/GNL is a key enzyme involved in vitamin C biosynthesis (5). To avoid the effects of vitamin C deficiency, L-(+)-ascorbic acid (vitamin C, 1.5 g/liter) and 10 μM EDTA were added to the drinking water. The water was changed every 3 d until the experiment ended. Mice had free access to water and food and were maintained on a 12-h light, 12-h dark cycle with a controlled temperature. All experimental procedures were approved by the Committee for Animal Research, Kyoto Prefectural University of Medicine.

Analytic procedures and glucose and insulin tolerance tests

Blood glucose levels were measured using a glucometer (Gultest Ace; Sanwa Kagaku Kenkyusho Co., Ltd., Nagoya, Japan). To measure plasma lipids, blood was collected by cardiac puncture after an overnight fast just before the tissue collection. Plasma nonesterified fatty acid (NEFA), triglycerides, and total cholesterol were measured by the enzymatic method using an autoanalyzer. Intraperitoneal glucose (2 g/kg body weight) and insulin (0.75 U/kg body weight) tolerance tests were performed after 16- and 7-h fasts, respectively, and blood glucose was measured at the time indicated. For insulin release during glucose tolerance testing, the plasma component of blood collected at the 0- and 30-min time points was measured with an insulin enzyme immunoassay system, the Morinaga ultrasensitive mouse insulin assay kit (Morinaga Institute of Biological Science, Inc., Kanagawa, Japan).

Tissue collection and histological assessment of pancreatic islets

After an overnight fast, mice were killed by administration of an overdose of sodium aminobarbital. After blood collection by cardiac puncture, the lateral epididymal and inguinal sc adipose tissue depots were removed and weighed. A portion of the liver was used for measurement of total vitamin C content.

The whole pancreas was removed, cleared of fat and lymph nodes, weighed, fixed in 10% formalin solution, and embedded in paraffin. Pancreatic sections were prepared and stained with hematoxylin and eosin or an antibody against insulin using the Histofine mouse stain kit with a mouse antihuman insulin antibody (Nichirei Biosciences Inc., Tokyo, Japan). For morphometric analysis of β-cell mass, pancreatic sections 250 μm apart taken from three different levels of the pancreatic tissue block (five pancreases per experimental group) were examined. Nonoverlapping images were captured with a digital camera (Sony DXC-S500/OL; Sony, Tokyo, Japan). The β-cell area and the section area were analyzed using NIH Image J version 1.36b software. The β-cell mass was calculated by multiplying the pancreas weight by the percentage of β-cell area per pancreas.

To evaluate cell replication per islet, we performed labeling of proliferating cells with the DNA precursor analog 5-bromo-2-deoxyuridine (BrdU). Mice were injected ip with BrdU (1 mg/mouse; BD Biosciences, San Diego, CA) 12 h before being killed. After tissue processing as described above, immunostaining for BrdU was performed with a BrdU *in situ* detection kit (BD Biosciences) (16). All visible islets for each pancreatic section (three sections per animal) were analyzed to determine the total number of BrdU-positive cells and total islet count per section.

Measurement of pancreatic insulin content

Pancreatic insulin content was determined as previously described (17). Briefly, a portion of the pancreatic tail was homogenized in acidic ethanol (0.18 mol/liter HCl in 95% ethanol) and was extracted for 24 h at 4 C. The homogenate was centrifuged at 2000 $\times$ *g* for 15 min. Insulin levels in the supernatant were assayed as described above.

Measurement of total vitamin C levels in the liver

Livers were homogenized in 14 vol 5.4% metaphosphate, and then the homogenate was centrifuged at 21,000 $\times$ *g* for 15 min

at 4 C. Ascorbic acid in samples was treated with 0.1% dithiothreitol to reduce the dehydroascorbic acid to ascorbic acid and was analyzed by HPLC using an Atlantis dC18 5-μm column (4.6 × 150 mm; Nihon Waters, Tokyo, Japan) (11). The mobile phase was 50 mM phosphate buffer (pH 2.8), 0.2 g/liter EDTA, and 2% methanol at a flow rate of 1.3 ml/min, and electrical signals were recorded by using an electrochemical detector with a glassy carbon electrode at +0.6 V.

Static insulin secretion from isolated islets

Male SD-fed SMP30/GNL KO mice and C57BL/6CrSlc mice (14–15 wk of age) were used for islets isolation. Islets were isolated using collagenase (type V collagenase; Sigma Chemical Co., St. Louis, MO), digested in Hanks' buffer, followed by separation of islets from exocrine tissue in a Histopaque (Histopaque 1077; Sigma) gradient (18). Islets of similar size were hand picked under a stereomicroscope into groups (n = 5) of five islets in triplicate. The islets were preincubated for 60 min at 37 C in Krebs-Ringer bicarbonate HEPES buffer (equilibrated with 95% O_2 and 5% CO_2, pH 7.4) supplemented with 2 mg/ml BSA (fraction V; Sigma) and 2 mM glucose. After preincubation, five islets were incubated with 200 μl of the same buffer for 15 min. After samples from the buffer were removed for measurement of insulin, the islets were incubated in the presence of 20 mM glucose or 20 mM KCl plus 2 mM glucose for another 15 min. At the end of this period, the supernatant was collected. All samples were stored at −80 C until the insulin assay (Morinaga ultrasensitive mouse insulin assay kit).

ATP measurement from isolated islets

Cultured islets were preincubated at 37 C for 60 min in Krebs-Ringer bicarbonate HEPES buffer with 2 mM glucose, and then triplicate batches of 10 islets were incubated at 2 or 20 mM glucose for another 60 min. ATP was extracted from islets according to the methods described by Uchizono *et al.* (19). ATP levels were measured using the Enliten ATP assay system (Promega, Madison, WI) with a bioluminometer (GloMax 20/20n luminometer; Promega).

Statistical analysis

The data are expressed as means ± SE. Significance was determined by one-way ANOVA with Dunn's multiple comparisons *post hoc* or unpaired Student's *t* test where appropriate. A two-way ANOVA was used to compare the glucose and insulin levels on the same time point in ip glucose tolerance test. A value of $P < 0.05$ was considered to be significant.

Results

Energy intake, body weight, and adipose tissue

The mean energy intakes of the WT mice fed a SD, WT mice fed a HFD, SMP30/GNL KO mice fed an SD, and SMP30/GNL KO mice fed an HFD throughout the study were 9.1 ± 0.1, 13.1 ± 0.2, 8.5 ± 0.1, and 11.8 ± 0.2 kcal/d, respectively. All four groups of mice gained weight; however, the increase in body weight in the HFD-fed WT and HFD-fed SMP30/GNL KO mice was significantly higher than that in SD-fed WT and SD-fed SMP30/GNL KO mice (Fig. 1). The weight gain in the SD-fed WT, SD-fed SMP30/GNL KO, HFD-fed WT, and HFD-fed SMP30/GNL KO mice after 8 wk on the diets was 8.4 ± 0.4, 8.2 ± 0.4, 16.5 ± 0.7, and 14.7 ± 0.7 g/mouse, respectively. The HFD-fed WT mice gained 51% more weight than the SD-fed WT mice, and HFD-fed SMP30/GNL KO mice gained 56% more weight than the SD-fed SMP30/GNL KO mice.

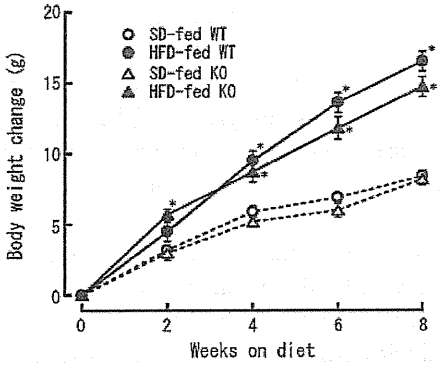

FIG. 1. Body weight changes of SD-fed and HFD-fed WT and SMP30/GNL KO mice. Experimental diets were started at 7 wk of age and continued for 8 wk (until 15 wk of age). *, $P < 0.01$ *vs.* SD-fed WT and SMP30/GNL KO mice. Data are means ± SE (n = 10 per group).

Epididymal fat pads from HFD-fed WT and HFD-fed SMP30/GNL KO mice after 8 wk on the diet were significantly heavier than fat pads from the SD-fed WT and SD-fed SMP30/GNL KO mice (Table 1). The ratio of epididymal fat mass to sc fat mass in HFD-fed WT and HFD-fed SMP30/GNL KO mice was also larger than in SD-fed WT and SD-fed SMP30/GNL KO mice, although the differences were not significant.

Total vitamin C levels in the liver

To examine the vitamin C status of the SMP30/GNL KO mice, we determined the total vitamin C content in the liver after 8 wk on the diets. The total vitamin C levels in the liver from SD-fed and HFD-fed WT mice and SD-fed and HFD-fed SMP30/GNL KO mice were 188.2 ± 12.3, 176.6 ± 8.9, 160.2 ± 7.4, and 150.4 ± 6.9 μg/g tissue, respectively. There were no significant differences among the four groups.

Blood glucose and plasma lipid levels

Fasting glucose levels of HFD-fed WT and HFD-fed SMP30/GNL KO mice after 8 wk on HFD were significantly increased in both groups compared with SD-fed WT and SD-fed SMP30/GNL KO mice (Table 1).

After 8 wk on HFD, HFD-fed WT and HFD-fed SMP30/GNL KO mice showed significant increases in total plasma cholesterol levels from 61–67% compared with SD-fed WT and SD-fed SMP30/GNL KO mice; however, there was no significant difference in plasma total

TABLE 1. Fasting glucose, plasma lipids, and adipose tissue weight after 8 wk on diet (15 wk of age)

	SD		HFD	
	WT	SMP30/GNL KO	WT	SMP30/GNL KO
Fasting glucose (mg/dl)	109.5 ± 3.7	101.6 ± 5.0	129.6 ± 6.4[a]	138.3 ± 6.7[a]
NEFA (mEq/liter)	1487.0 ± 79.0	1439.2 ± 56.6	927.9 ± 40.6[a]	882.1 ± 39.8[a]
Triglycerides (mg/dl)	106.4 ± 3.2	93.8 ± 4.5	74.6 ± 5.4[a]	69.8 ± 4.8[a]
Total cholesterol (mg/dl)	117.3 ± 2.7	108.1 ± 2.4	191.5 ± 10.2[b]	161.5 ± 6.6[a]
Epididymal fat (mg/g BW)	12.6 ± 1.5	9.0 ± 1.0	23.5 ± 1.9[a]	18.8 ± 2.1[a]
sc fat (mg/g BW)	5.9 ± 1.1	3.3 ± 0.5[b]	7.5 ± 0.5	5.5 ± 0.4
Epi/Sub	2.5 ± 0.4	2.9 ± 0.3	3.3 ± 0.4	3.4 ± 0.3

Data are means ± SE from 10 mice. BW, Body weight; Epi/Sub, ratio of epididymal fat mass to sc fat mass.

[a] $P < 0.05$ *vs.* SD-fed WT and SMP30/GNL KO mice.

[b] $P < 0.05$ *vs.* the other three groups.

cholesterol levels between SD-fed WT and SD-fed SMP30/GNL KO mice (Table 1). Compared with the mice fed SD, mice fed HFD had lower triglyceride and NEFA levels. However, there was no difference in triglyceride and NEFA levels between WT and SMP30/GNL KO mice. This paradoxical decrease in triglycerides and NEFAs is consistent with a previous report showing that the C57BL/6 strain has a unique metabolic response to HFD (20). These data indicate that deficiency of SMP30 has no influence on lipid profile either in SD-fed or in HFD-fed animal.

Intraperitoneal glucose tolerance test

Blood glucose levels at 30 min after glucose administration were 25% higher in SD-fed SMP30/GNL KO mice than in SD-fed WT mice ($P < 0.05$, Fig. 2A). And blood glucose levels at 30, 60, and 120 min after glucose administration were significantly higher in HFD-fed WT and HFD-fed SMP30/GNL KO mice than in SD-fed WT and SD-fed SMP30/GNL KO mice. Moreover, the blood glucose levels of HFD-fed SMP30/GNL KO mice at 60 and 120 min after glucose administration were significantly higher than those of HFD-fed WT mice. The areas under the curve (AUC, 0–120 min) in SD-fed and HFD-fed WT mice and SD-fed and HFD-fed SMP30/GNL KO mice were 417.1 ± 18.3, 721.2 ± 41.7, 496.1 ± 36.2, and 900.2 ± 40.6 mg · h/dl, respectively (ANOVA, $P < 0.0001$). It is noteworthy that the AUC did not differ between SD-fed WT and SD-fed SMP30/GNL KO mice ($P = 0.128$). This result indicates that the significantly high blood glucose levels appeared restrictively at 30 min after glucose administration in SD-fed SMP30/GNL KO mice.

There were no significant differences in fasting insulin levels between SD-fed WT and SD-fed SMP30/GNL KO mice (Fig. 2B). However, insulin levels of SD-fed SMP30/GNL KO mice at 30 min after glucose were 37% lower than those of SD-fed WT mice ($P < 0.05$). HFD feeding increased fasting insulin levels in both WT and SMP30/GNL KO mice; however, those of SMP30/GNL KO mice were 39% lower than those of WT mice. Similarly, insulin levels at 30 min after glucose were 27% lower in HFD-fed SMP30/GNL KO mice compared with those of HFD-fed WT mice. The AUC (0–30 min) in SD-fed and HFD-fed WT mice and SD-fed and HFD-fed SMP30/GNL KO mice were 1.09 ± 0.08, 1.86 ± 0.19, 0.71 ± 0.11, and 1.19 ± 0.12 ng · 30 min/ml, respectively (ANOVA, $P < 0.0001$). The AUC in SD-fed SMP30/GNL KO mice was lower than that in SD-fed WT mice, although the difference was not statistically significant ($P = 0.052$).

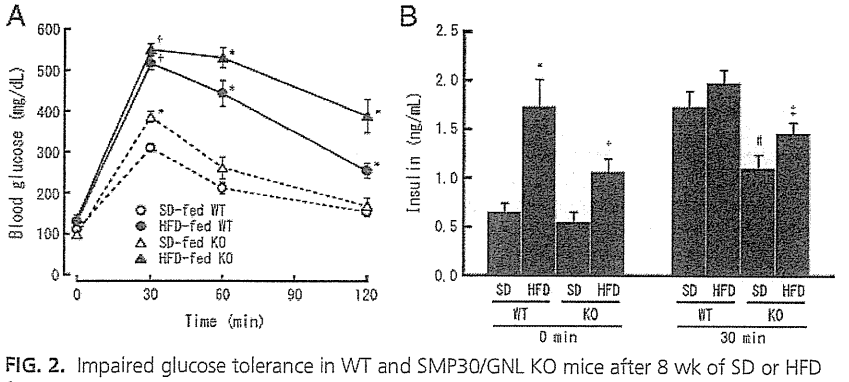

FIG. 2. Impaired glucose tolerance in WT and SMP30/GNL KO mice after 8 wk of SD or HFD feeding. A, Intraperitoneal glucose tolerance test; B, insulin levels at baseline and at 30 min after glucose. *, $P < 0.05$ *vs.* the other three groups; †, $P < 0.05$ *vs.* SD-fed WT and SMP30/GNL KO mice; #, $P < 0.05$ *vs.* SD-fed and HFD-fed WT mice; ‡, $P < 0.05$ *vs.* HFD-fed WT mice. Data are means ± SE (n = 7 per group).

Insulin tolerance test

We next assessed insulin sensitivity using an insulin tolerance test. Blood glucose levels in SD-fed SMP30/GNL KO mice were significantly reduced to 49 and 51% of the levels of SD-fed WT mice after 30 and 60 min, respectively, indicating high peripheral insulin sensitivity (Fig. 3). HFD-fed SMP30/GNL KO mice showed similar insulin tolerance to that of SD-fed WT mice.

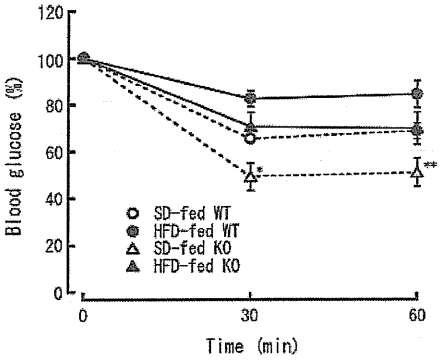

FIG. 3. Intraperitoneal insulin tolerance test after 8 wk of SD or HFD feeding. Data are expressed as percentage of basal (0 min) glucose levels. *, $P < 0.05$ *vs.* HFD-fed WT and SMP30/GNL KO mice; **, $P < 0.05$ *vs.* the other three groups. Data are means ± SE (n = 7 per group).

β-Cell mass and proliferation

The pancreas weight per body weight was significantly lower in SD-fed SMP30/GNL KO mice than in SD-fed WT mice (Table 2). Eight weeks of HFD feeding increased the pancreas weight of SMP30/GNL KO mice to the same level as SD-fed and HFD-fed WT mice. Morphometric analyses of β-cell mass, as assessed by immunohistochemical analysis, revealed no differences between SMP30/GNL KO mice and WT mice (Table 2). HFD feeding significantly increased β-cell mass in both WT and SMP30/GNL KO mice to similar levels. Similarly, there were no significant differences in pancreatic insulin content in response to HFD feeding between WT and SMP30/GNL KO mice (Table 2).

Hematoxylin and eosin staining revealed no differences in islet morphology among the four groups. The proliferation of islet cells, which was determined by the frequency of BrdU-positive cells per islet, in both HFD-fed WT and SMP30/GNL KO mice was significantly higher than in animals fed SD (Fig. 4 and Table 2). In addition, there was no difference in islet proliferation between SMP30/GNL KO and WT mice. This finding demonstrates that the proliferation of β-cells to compensate for increased insulin demand is not impaired in SMP30/GNL KO mice. However, insulin levels of SD-fed SMP30/GNL KO mice at 30 min after glucose were 37% lower than those of SD-fed WT mice.

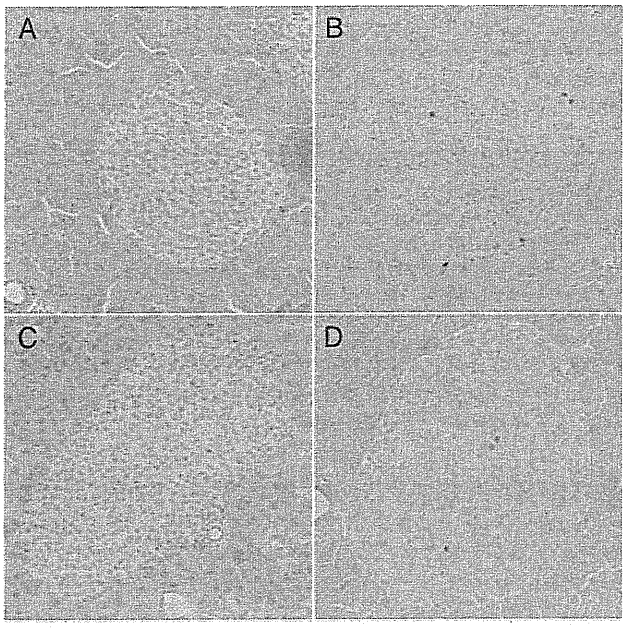

FIG. 4. Immunohistochemical staining of BrdU in pancreas sections. Mice were injected with BrdU 12 h before being killed. BrdU-positive cells (*brown*) were observed in the islets of both WT (B) and SMP30/GNL KO mice (D) on the HFD. A and C, WT (A) and SMP30/GNL KO mice (C) on the SD. Magnification, ×100.

Insulin secretion and ATP measurements from isolated islets

To confirm β-cell dysfunction in SMP30/GNL KO mice, we measured insulin secretion in response to glucose and KCl from the isolated islets. The basal insulin secretion in SD-fed SMP30/GNL KO and WT mice were 89.3 ± 9.8 and 93.3 ± 10.4 pg/islet · 15 min (n = 10), respectively. There were no significant differences between the two. Similar to *in vivo* results, insulin secretion of SD-fed SMP30/GNL KO mice in 20 mM glucose for 15 min was significantly reduced compared with those of SD-fed WT mice ($P < 0.05$, Fig. 5A). Insulin secretory response to 20

TABLE 2. Morphometric analysis and insulin contents of pancreases after 8 wk of SD or HFD feeding

	Pancreas weight (mg/g body weight), n = 10	Pancreatic insulin content (μg/g pancreas), n = 10	β-Cell mass (mg), n = 5	BrdU index (%), n = 5
SD				
WT	5.4 ± 0.4	42.1 ± 3.9	1.21 ± 0.21	4.4 ± 2.8
SMP30/GNL KO	4.1 ± 0.2[a]	40.4 ± 4.6	1.14 ± 0.13	6.9 ± 3.5
HFD				
WT	5.4 ± 0.2	56.7 ± 4.9[b]	3.28 ± 0.85[b]	37.3 ± 11.7[b]
SMP30/GNL KO	5.6 ± 0.4	53.1 ± 4.1[b]	2.83 ± 0.41[b]	47.3 ± 10.6[b]

BrdU index: total BrdU positive islet cells/total islet counts per section.

[a] $P < 0.05$ *vs.* the other three groups.

[b] $P < 0.05$ *vs.* SD-fed WT and SMP30/GNL KO mice.

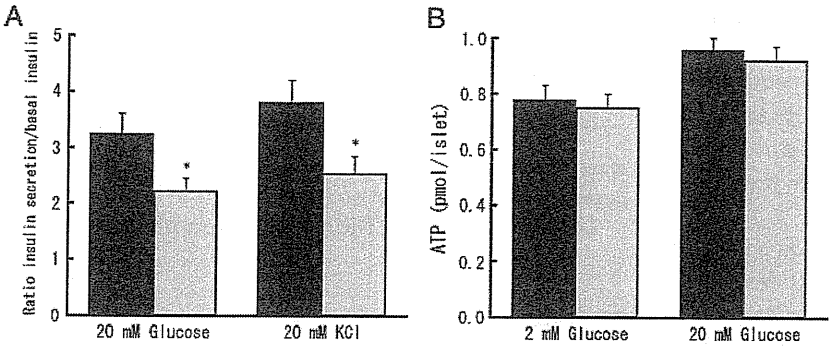

FIG. 5. Insulin secretion and ATP content in islets isolated from WT (*black bars*) and SD-fed SMP30/GNL KO mice (*gray bars*) (14–15 wk of age). A, Static islet incubation for 15 min in 20 mM glucose or 20 mM KCl. The data are expressed as ratio of 15 min to basal insulin (picograms per islet per 15min). *, $P < 0.05$ *vs.* WT mice. Data are means ± SE (n = 5 per group). B, ATP content at 2 and 20 mM glucose. There were no significant differences in ATP content at 2 or 20 mM glucose between WT and SMP30/GNL KO mice. Data are means ± SE (n = 5 per group).

mM KCl was also reduced significantly in SMP30/GNL KO mice ($P < 0.05$, Fig. 5A).

Islet ATP content was significantly elevated at 20 mM glucose compared with 2 mM glucose in SD-fed SMP30/GNL KO and WT mice. However, there were no significant differences in ATP content at 2 or 20 mM glucose between the two (Fig. 5B).

Discussion

This is the first report documenting impaired glucose tolerance in SMP30/GNL-deficient mice and provides new insight into the possible role of SMP30/GNL in glucose homeostasis. Our *in vitro* data using isolated islets confirmed that deletion of SMP30/GNL was responsible for the reduced insulin secretory response to glucose. The present study differs from previous studies using SMP30/GNL KO mice, in that the mice were maintained with a sufficient supply of vitamin C. This eliminated the confounding secondary effects of vitamin C on glucose homeostasis and made this experimental model more relevant to human disease.

SMP30/GNL KO mice at 15 wk of age demonstrated mild glucose intolerance compared with WT mice. They also showed an impairment in acute insulin secretion after glucose administration and better peripheral insulin sensitivity as assessed by an insulin tolerance test. These data suggest that an impairment of the early phase of insulin secretion underlies the glucose intolerance seen in SMP30/GNL KO mice. In HFD-fed WT mice as well as in SMP30/GNL KO mice, HFD feeding increased fat mass and worsened glucose tolerance. However, this impairment of glucose tolerance was more pronounced in SMP30/GNL KO mice. This difference likely reflects SMP30/GNL KO mice's intrinsic reduction in insulin secretion capacity, as shown by their impaired acute insulin secretion after a glucose load and similar insulin resistance to WT mice when fed an HFD. It has been reported that vitamin C treatment has no effect on insulin secretion in diabetic C57BL/KsJ-db/db mice or nondiabetic control mice (21). Thus, the differential vitamin C status seen in this study is unlikely to be the cause of the impairment of insulin secretion.

It is interesting that SMP30/GNL KO mice had the higher peripheral insulin sensitivity. The better insulin sensitivity might partially compensate for the decreased insulin secretion and made the moderate impairment of glucose tolerance. Although the present data could not refer to its mechanism, the lower epididymal and sc fat mass in SMP30/GNL KO mice may help account for the result. Now, we can just assume that absence of SMP30/GNL in insulin-sensitive tissues, including liver, kidney, fat, and muscle, may directly affect insulin signaling pathway or secondarily affect insulin action through metabolic pathways. Also, an increased insulin clearance from the liver is another possibility. It is well known that increased insulin resistance is a major factor involved in impaired glucose tolerance in the elderly. So we would say that SMP30/GNL KO mice is not an appropriate animal model of impaired glucose tolerance in normal aging.

The static incubation study of islets demonstrated the reduced insulin secretory response to glucose and KCl in SMP30/GNL-deficient mice. KCl depolarizes the β-cell plasma membrane, which initiates a series of events such as Ca^{2+} influx, mobilization of Ca^{2+} from intracellular stores, and insulin exocytosis. On the other hand, glucose-stimulated insulin secretion from the β-cell occurs after generation of ATP from metabolism of glucose through glycolysis and the Krebs cycle. The intracellular rise in ATP/ADP ratio leads to closure of the K_{ATP} channels, Ca^{2+} influx, and subsequent activation of insulin secretion. The reduced insulin secretory response to KCl, together with the preservation of ATP production, suggests that events in the distal portion of the insulin secretion pathway are impaired in SMP30/GNL-deficient mice. The mechanism underlying β-cell dysfunction in SMP30/GNL KO mice has not been fully explored. However, previous reports have proposed the possibility of dysregulation of Ca^{2+} homeostasis. SMP30/GNL maintains Ca^{2+} homeostasis by enhancing plasma membrane Ca^{2+}-pumping activity (3, 4). Therefore, taken together with the present results of *in vitro* islet study, a deficiency of SMP30/GNL

may induce dysregulation of Ca^{2+} homeostasis, resulting in impairment of the increase in Ca^{2+} influx resulting from a high glucose concentration and of Ca^{2+}-dependent signaling pathways, which are involved in the mechanisms of insulin secretion. Additional studies, such as intracellular calcium levels in β-cells may allow for a more precise localization of these abnormalities.

It has been well documented that HFD feeding induces compensatory β-cell hyperplasia in response to insulin resistance in mice (22, 23). In the present study, too, HFD feeding caused insulin resistance in both WT and SMP30/GNL KO mice, but there were no differences in the degree of compensatory increase in β-cell mass and proliferation between WT and SMP30/GNL KO mice. These findings suggest that SMP30/GNL deficiency causes β-cell dysfunction without impairment of the mechanism responsible for islet hyperplasia.

Both decreased insulin secretion and increased insulin resistance are two major factors involved in impaired glucose tolerance in the elderly. Increased adiposity and decreased physical activity contribute to insulin resistance in the elderly (15). Recent reports indicate that the age-associated decline in muscle mitochondrial function is a mechanism for insulin resistance (24). On the other hand, the molecular mechanism for the development of age-dependent β-cell defects is still unknown. Aging could be associated with a loss of β-cell mass or impaired β-cell function or a combination of these two factors (25–27). The present results suggest the possibility that a reduction in SMP30/GNL with age contributes to the age-related impairment of β-cell function. If this is the case, SMP30/GNL could be a novel molecule that is involved not only in the impaired insulin secretion that occurs with normal aging but also in the pathogenesis of type 2 diabetes.

In summary, SMP30/GNL KO mice have modestly impaired glucose tolerance with an impairment of acute insulin secretion due to dysfunction of the distal portion of the secretion pathway. The increase in β-cell mass and proliferation to compensate for insulin resistance is equivalent to that of WT mice. The present results suggest that reduction in SMP30/GNL could be a factor that contributes to the worsening of glucose tolerance with normal aging and that this mechanism may provide new insights into the age-associated pathophysiology of β-cell function.

Acknowledgments

We thank Fumie Takenaka, Hiroko Kawamura, and Sayoko Horibe for their secretarial assistance. Vitamin C powder was kindly provided by DSM Nutrition Japan (Tokyo, Japan).

Address all correspondence and requests for reprints to: Goji Hasegawa, M.D., Department of Endocrinology and Metabolism, Kyoto Prefectural University of Medicine Graduate School of Medical Science, 465 Kajii-cho, Hirokoji, Kawaramachi-dori, Kamikyo-ku, Kyoto 602-8566, Japan. E-mail: goji@koto.kpu-m.ac.jp.

This work was supported by Grants-in-Aid for Scientific Research (20591066 to G.H. and 18590355 to A.I.) from the Japan Society for the Promotion of Science.

Disclosure Summary: The authors have nothing to disclose.

References

1. Fujita T, Uchida K, Maruyama N 1992 Purification of senescence marker protein-30 (SMP30) and its androgen-independent decrease with age in the rat liver. Biochim Biophys Acta 1116:122–128
2. Ishigami A, Maruyama N 2007 Significance of SMP30 in gerontology. Geriatr Gerontol Int 7:316–325
3. Fujita T, Inoue H, Kitamura T, Sato N, Shimosawa T, Maruyama N 1998 Senescence marker protein-30 (SMP30) rescues cell death by enhancing plasma membrane Ca^{2+}-pumping activity in Hep G2 cells. Biochem Biophys Res Commun 250:374–380
4. Inoue H, Fujita T, Kitamura T, Shimosawa T, Nagasawa R, Inoue R, Maruyama N, Nagasawa T 1999 Senescence marker protein-30 (SMP30) enhances the calcium efflux from renal tubular epithelial cells. Clin Exp Nephr 3:261–267
5. Kondo Y, Inai Y, Sato Y, Handa S, Kubo S, Shimokado K, Goto S, Nishikimi M, Maruyama N, Ishigami A 2006 Senescence marker protein 30 functions as gluconolactonase in L-ascorbic acid biosynthesis, and its knockout mice are prone to scurvy. Proc Natl Acad Sci USA 103:5723–5728
6. Ishigami A, Fujita T, Handa S, Shirasawa T, Koseki H, Kitamura T, Enomoto N, Sato N, Shimosawa T, Maruyama N 2002 Senescence marker protein-30 knockout mouse liver is highly susceptible to tumor necrosis factor-α- and Fas-mediated apoptosis. Am J Pathol 161:1273–1281
7. Ishigami A, Kondo Y, Nanba R, Ohsawa T, Handa S, Kubo S, Akita M, Maruyama N 2004 SMP30 deficiency in mice causes an accumulation of neutral lipids and phospholipids in the liver and shortens the life span. Biochem Biophys Res Commun 315:575–580
8. Mori T, Ishigami A, Seyama K, Onai R, Kubo S, Shimizu K, Maruyama N, Fukuchi Y 2004 Senescence marker protein-30 knockout mouse as a novel murine model of senile lung. Pathol Int 54:167–173
9. Sato T, Seyama K, Sato Y, Mori H, Souma S, Akiyoshi T, Kodama Y, Mori T, Goto S, Takahashi K, Fukuchi Y, Maruyama N, Ishigami A 2006 Senescence marker protein-30 protects mice lungs from oxidative stress, aging, and smoking. Am J Respir Crit Care Med 174:530–537
10. Son TG, Zou Y, Jung KJ, Yu BP, Ishigami A, Maruyama N, Lee J 2006 SMP30 deficiency causes increased oxidative stress in brain. Mech Ageing Dev 127:451–457
11. Furusawa H, Sato Y, Tanaka Y, Inai Y, Amano A, Iwama M, Kondo Y, Handa S, Murata A, Nishikimi M, Goto S, Maruyama N, Takahashi R, Ishigami A 2008 Vitamin C is not essential for carnitine biosynthesis in vivo: verification in vitamin C-depleted senescence marker protein-30/gluconolactonase knockout mice. Biol Pharm Bull 31:1673–1679
12. Kondo Y, Sasaki T, Sato Y, Amano A, Aizawa S, Iwama M, Handa S, Shimada N, Fukuda M, Akita M, Lee J, Jeong KS, Maruyama N, Ishigami A 2008 Vitamin C depletion increases superoxide generation in brains of SMP30/GNL knockout mice. Biochem Biophys Res Commun 377:291–296
13. Sato Y, Kajiyama S, Amano A, Kondo Y, Sasaki T, Handa S, Takahashi R, Fukui M, Hasegawa G, Nakamura N, Fujinawa H, Mori T, Ohta M, Obayashi H, Maruyama N, Ishigami A 2008 Hydrogen-rich pure water prevents superoxide formation in brain

slices of vitamin C-depleted SMP30/GNL knockout mice. Biochem Biophys Res Commun 375:346–350
14. Chang AM, Halter JB 2003 Aging and insulin secretion. Am J Physiol Endocrinol Metab 284:E7–E12
15. Scheen AJ 2005 Diabetes mellitus in the elderly: insulin resistance and/or impaired insulin secretion? Diabetes Metab 31(Spec No 2): 5S27–25S34
16. Robertson H, Wheeler J, Morley AR 1990 In vivo bromodeoxyuridine incorporation in normal mouse kidney: immunohistochemical detection and measurement of labelling indices. Histochem J 22: 209–214
17. Hasegawa G, Mori H, Sawada M, Takagi S, Shigeta H, Kitagawa Y, Nakano K, Kanatsuna T, Kondo M 1990 Dietary treatment ameliorates overt diabetes and decreased insulin secretion to glucose induced by overeating in impaired glucose tolerant mice. Horm Metab Res 22:408–412
18. Lacy PE, Kostianovsky M 1967 Method of the isolation of intact islets of Langerhans from the rat pancreas. Diabetes 16:35–39
19. Uchizono Y, Iwase M, Nakamura U, Sasaki N, Goto D, Iida M 2004 Tacrolimus impairment of insulin secretion in isolated rats islets occurs at multiple distal sites in stimulus-secretion coupling. Endocrinology 145:2264–2272
20. Colombo C, Haluzik M, Cutson JJ, Dietz KR, Marcus-Samuels B, Vinson C, Gavrilova O, Reitman ML 2003 Opposite effects of background genotype on muscle and liver insulin sensitivity of lipoatrophic mice. Role of triglyceride clearance. J Biol Chem 278:3992–3999
21. Kaneto H, Kajimoto Y, Miyagawa J, Matsuoka T, Fujitani Y, Umayahara Y, Hanafusa T, Matsuzawa Y, Yamasaki Y, Hori M 1999 Beneficial effects of antioxidants in diabetes: possible protection of pancreatic β-cells against glucose toxicity. Diabetes 48:2398–2406
22. Sone H, Kagawa Y 2005 Pancreatic β-cell senescence contributes to the pathogenesis of type 2 diabetes in high-fat diet-induced diabetic mice. Diabetologia 48:58–67
23. Terauchi Y, Takamoto I, Kubota N, Matsui J, Suzuki R, Komeda K, Hara A, Toyoda Y, Miwa I, Aizawa S, Tsutsumi S, Tsubamoto Y, Hashimoto S, Eto K, Nakamura A, Noda M, Tobe K, Aburatani H, Nagai R, Kadowaki T 2007 Glucokinase and IRS-2 are required for compensatory β-cell hyperplasia in response to high-fat diet-induced insulin resistance. J Clin Invest 117:246–257
24. Petersen KF, Befroy D, Dufour S, Dziura J, Ariyan C, Rothman DL, DiPietro L, Cline GW, Shulman GI 2003 Mitochondrial dysfunction in the elderly: possible role in insulin resistance. Science 300:1140–1142
25. Chang AM, Smith MJ, Galecki AT, Bloem CJ, Halter JB 2006 Impaired β-cell function in human aging: response to nicotinic acid-induced insulin resistance. J Clin Endocrinol Metab 91:3303–3309
26. Maedler K, Schumann DM, Schulthess F, Oberholzer J, Bosco D, Berney T, Donath MY 2006 Aging correlates with decreased β-cell proliferative capacity and enhanced sensitivity to apoptosis: a potential role for Fas and pancreatic duodenal homeobox-1. Diabetes 55:2455–2462
27. Szoke E, Shrayyef MZ, Messing S, Woerle HJ, van Haeften TW, Meyer C, Mitrakou A, Pimenta W, Gerich JE 2008 Effect of aging on glucose homeostasis: accelerated deterioration of β-cell function in individuals with impaired glucose tolerance. Diabetes Care 31: 539–543